Improved Caps for Improved Subdivision Surfaces

Kęstutis Karčiauskas[a], Jörg Peters[b,*]

Department CISE, University of Florida

[a] *Vilnius University, Lithuania*
[b] *University of Florida, USA*

Abstract

The quest for a finite number of bicubic (bi-3) polynomial pieces to smoothly fill multi-sided holes after a fixed number of surface subdivision steps has motivated a number of constructions of finite surface caps. Recent bi-3 and bi-4 subdivision algorithms have improved surface shape compared to classic Catmull-Clark and curvature-bounded 'tuned' subdivision. Since the older subdivision algorithms exhibit artifacts that obscure the shortcomings of corresponding caps, it is worth re-visiting their multi-sided fill surfaces. The improved caps address the challenge so that either bi-3 or bi-4 data can be accommodated, as needed. The derivation illustrates the subtle fundamental trade off between formal algebraic mathematical smoothness constraints and good shape in the large.

Keywords: subdivision surface, finitely-many patches, surface shape, smoothness

1. Introduction

For computer-aided design, an infinite sequence of surface rings as in Fig. 1 b is not just impractical but complicates downstream operations such as computing exact integrals, moments, and deformation under force. This motivates investigating how to smoothly cap multi-sided holes after a fixed number of subdivision steps. While, for visual effects, covering the hole with a triangle fan may suffice, geometric design aims to fill with a cap of the same high quality as the surrounding surface. Given recent improvements of subdivision surfaces, shortcomings in the existing panoply of caps become more visible (see Fig. 3). Since caps have to respond to different objectives: uniform highlight lines, exact C^1 transitions, low degree or low number of pieces, capping a bi-4 or bi-3 subdivision sequence of rings, we present a family of options to cater towards the desired set of properties, see Fig. 2 . The common ancestor, cap$^{\text{aux}}$, consists of n patches of degree bi-4 that provide good initial shape and approximate first-order Hermite data of the innermost subdivision ring.

New splits and reparameterizations improve formal smoothness and lower the polynomial degree. This completeness of options to address the variety of needs with new types of macro-patch layouts is the main contribution: older caps require transitions that introduce shape artifacts.

While 'tuned' subdivision algorithms, like [3], have a control net of the type Fig. 1 a, just like their classical ancestor [1] and multi-sided constructions, see e.g. [7], recent high-quality subdivision algorithms take advantage of a slightly different control net that can be obtained from Fig. 1 a by the conversion explained in [4, Eqs 1,2], respectively [2, Sect 3]. This net also provides a regular bi-cubic ring that surrounds the cap and so allows judging the quality of the transition from regular bi-3 splines to the cap. The first r subdivision steps generate a sequence of r contracting rings as illustrated in Fig. 1 b. Catmull-Clark [1] generates three bi-cubic patches per sector of such a ring, [2] three bi-4 patches.

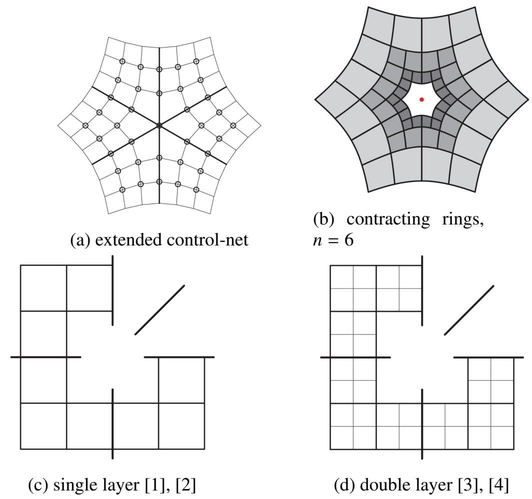

Figure 1: (a) Catmull-Clark input control net plus one layer of control points. (b) A nested sequence structure of subdivision rings with central limit point $\mathbf{c}_0$ shown as •: (c) single layer ring, (d) double-layer (macro-patch) ring. Each ring consists of an L-shaped collection of patches in each of the n sectors.

Both cases are illustrated by Fig. 1 c. [3] and [4] both produce three 2×2 bi-3 macro-patches per sector, as sketched in Fig. 1 d. The family of caps addresses all such types of subdivision rings. To judge the quality of the transition and the cap, note that in Fig. 3 we zoom into a small area around the cap and display highlight lines [8]. Evidently, an object-level view of a large, complex surface would prevent any serious analysis of surface artifacts.

Overview After a focused literature review in Section 2, Section 3 introduces the toolkit for *deriving* the caps. Since this section is necessarily technical, some readers may want to skip ahead to Fig. 8 (b), Fig. 10 (a), Fig. 12 (b), Fig. 15 (a) to take in the structure of the caps and appreciate the executive summary of Fig. 2 . Section 4 defines the progenitor bi-4 cap$^{\text{aux}}$ and the smooth completion cap$^{\boxplus}$. (We adhere strictly to the cap-with-superscript notation to avoid confusion between the constructions.) Section 5 derives the bi-3 $\widetilde{\text{cap}}^{\boxplus}$, $\widetilde{\text{cap}}^{9}$ and cap^{9},

*Corresponding author
Email addresses: kestutis.karciauskas@mif.vu.lt (Kęstutis Karčiauskas), jorg.peters@gmail.com (Jörg Peters)

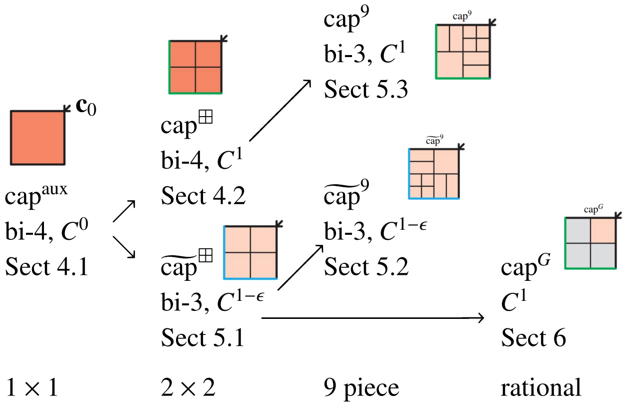

Figure 2: Genealogy of improved caps for improved subdivision surfaces. Icons depict one of n sectors of the cap. The central point $\mathbf{c}_0$ is always in the upper right hand corner. Cyan lower left edges of sector sketches indicate a $C^{1-\epsilon}$ transition, i.e. a tiny normal mismatch, from the last subdivision surface ring to the cap. Green boundaries indicate a proper C^1 transition. Internally, all cap sectors are C^1 and adjacent sectors are G^1 connected. Bi-4 patches are brick red, bi-3 pink; gray indicates Gregory-type patches with 4×4 coefficients, some of which are rational expressions in u, v. (The true rational degree of $\mathrm{cap}^G$is bi-7.)

and Section 6 defines the Gregory type rational cap^G. Notably, the implementations amount to assembling a matrix and multiplying it by the input control structure $[\mathbf{c}_0, \mathbf{d}^s_{ij}]$ consisting of a central point $\mathbf{c}_0$ and the net $\mathbf{d}$ that encapsulates the first-order Hermite data across the boundary of the innermost subdivision ring. Focusing on the interplay of smoothness, surface quality, polynomial degree and layout complexity, Section 7 compares the caps to alternatives and each other and shows that transitions to accommodate older cap constructions harm surface quality.

2. Prior work

Alignment of patch boundaries with features for better shape and fundamental facts of topology imply that control nets of free form surfaces with quadrilateral facets must allow for nodes with $n \neq 4$ neighbors. Looking at this challenge in general, a large number of solutions of good shape, measured as uniform highlight line distribution [8], exist in the literature, e.g. the curvature continuous polynomial constructions of degree bi-7 [9] of degree bi-6 [10], rational blending constructions [11, 12], curved knot-line splines [13] and manifold splines [14]. Here we focus on geometrically continuous spline caps (G-spline caps) that assemble a finite number of polynomial pieces to join smoothly after a change of variables. For downstream processing and uniformity of polynomial degree, constructions of lower degree are advantageous. A number of constructions of degree as low as bi-3 solve the algebraic smoothness constraints [15, 16, 17] but do not necessarily yield surfaces with acceptable highlight line distributions. Conversely, several publication focus on empirically good highlight lines. Examples of bi-5 caps are [18] and the macro-patch bi-4 caps of [19] and [7] developed to serve both geometry and solving partial differential equations on the geometry. There are even bi-3 caps with very small normal mismatch, called $C^{1-\epsilon}$ (almost C^1) constructions: the surfaces of [20] do not match the rings of an improved subdivision ring, but serves as inspiration for $\widetilde{\mathrm{cap}}^{\boxplus}$ and $\widetilde{\mathrm{cap}}^9$. The construction of $\mathrm{cap}^{\mathrm{aux}}$ is akin to the bi-4 cap construction in [21], whereas cap^G is a new variant of the classical Gregory-patch approach [22] but different from [23] and the rational multi-sided surfaces of [24, 12].

The recent subdivision surfaces [4] and [2] build on the idea of guided subdivision. They improve on the arguably best-optimized (tuned) subdivision eigen-expansion of [3]. However, in contrast to [25] these recent subdivision surfaces have the construction of a guide surface built into their explicit refinement stencils.

Hybrids of a finite number of subdivision rings completed with a cap are particularly useful as the final stage of nestedly refining spaces for use in engineering analysis. The finite polynomial formulation yields exact volume and moment formulas [26] and simplifies the integration compared even to optimized subdivision [27]. Realistically, six steps of subdivision suffice for such applications; and the C^1 or C^2 transitions between subdivision rings are simpler to work with than G^1 refinable constructions (see [28]). Section 7 illustrates why many of mentioned schemes fail to complete high-quality subdivision surfaces maintaining the high quality.

3. Tools of the cap maker

To define cap constructions that work both for bi-3 and bi-4 subdivision, the input net is not assumed to be the classical Catmull-Clark control net of $6n+1$ nodes shown in Fig. 1 a, but a more general control net (that can be generated from the classical control net if needed) that consists of $12n + 1$ nodes $[\mathbf{c}_0, \mathbf{d}^s_{ij}]$ as explained in Section 3.2. The output surface is represented in BB-form, see Section 3.1. All caps can be generated by applying a large sparse matrix to the input net to yield the BB-coefficients of the output cap. Given the Hermite data $\mathbf{t}$ derived from the input data in Section 3.2, G^1 smoothness between adjacent sectors of a cap and with respect to target points obtained from an auxiliary bi-4 surface are explained in Section 3.3.

3.1. *Output surface representation* $\mathbf{p}$ *and jets of type* $\mathbf{j}_{k\times l}$

The rings of subdivision surfaces and the cap can be represented as tensor-product patches of bi-degree d in Bernstein-Bézier form (BB-form, [29, 30]). That is, for Bernstein polynomials $B^d_k(t) := \binom{d}{k}(1-t)^{d-k}t^k$,

$$\mathbf{p}(u, v) := \sum_{i=0}^{d}\sum_{j=0}^{d} \mathbf{p}_{ij} B^d_i(u) B^d_j(v), \quad 0 \le u, v \le 1.$$

Connecting the *BB-coefficients* $\mathbf{p}_{ij} \in \mathbb{R}^3$ to $\mathbf{p}_{i+1,j}$ and $\mathbf{p}_{i,j+1}$ wherever well-defined yields the *BB-net*. In this paper we construct the caps of bi-degree $d = 3$ (bi-3) and $d = 4$ (bi-4) to complete C^2 subdivision surfaces of degree bi-3 or bi-4. Fig. 4 demonstrates how BB-subnets $\mathbf{j}_{3\times 3}$ assemble to form bi-4 patches.

3.2. *Hermite data* $\mathbf{t}$ *and the input data* $[\mathbf{c}_0, \mathbf{d}^s_{ij}]$

For C^2 bi-4 subdivision surfaces with the layout of Fig. 1 c and C^2 bi-3 subdivision surface with the layout of Fig. 1 d, first-order Hermite prolongation of the finest subdivision ring along each boundary curve are expressed as the tensor-borders $\mathbf{t}$ (bi-4) and $\bar{\mathbf{t}}^0$, $\bar{\mathbf{t}}^1$ (bi-3), see Fig. 5 a,b. There is a natural one-to-one correspondence between a pair $\bar{\mathbf{t}}^0$, $\bar{\mathbf{t}}^1$ and $\mathbf{t}$ that preserves, at the two end-points $\bar{\mathbf{t}}^0_{00}$ and $\bar{\mathbf{t}}^0_{30}$, marked as big • in Fig. 5 , the 3×2 Hermite data $\begin{pmatrix} \partial_v f & \partial_u\partial_v f & \partial^2_u\partial_v f \\ f & \partial_u f & \partial^2_u f \end{pmatrix}$: the end-point jets $\mathbf{j}_{3\times 2}$ are scaled by 2 in each variable and presented in bi-4 form by applying the process of Fig. 4 . Explicitly, since for $j = 0, 1$,

$$\bar{\mathbf{t}}^1_{0j} := \bar{\mathbf{t}}^0_{3j}, \bar{\mathbf{t}}^0_{2j} := \bar{\mathbf{t}}^0_{3j} + \frac{1}{4}(\bar{\mathbf{t}}^0_{1j} - \bar{\mathbf{t}}^1_{2j}), \bar{\mathbf{t}}^1_{1j} := \bar{\mathbf{t}}^0_{3j} - \frac{1}{4}(\bar{\mathbf{t}}^0_{1j} - \bar{\mathbf{t}}^1_{2j}),$$

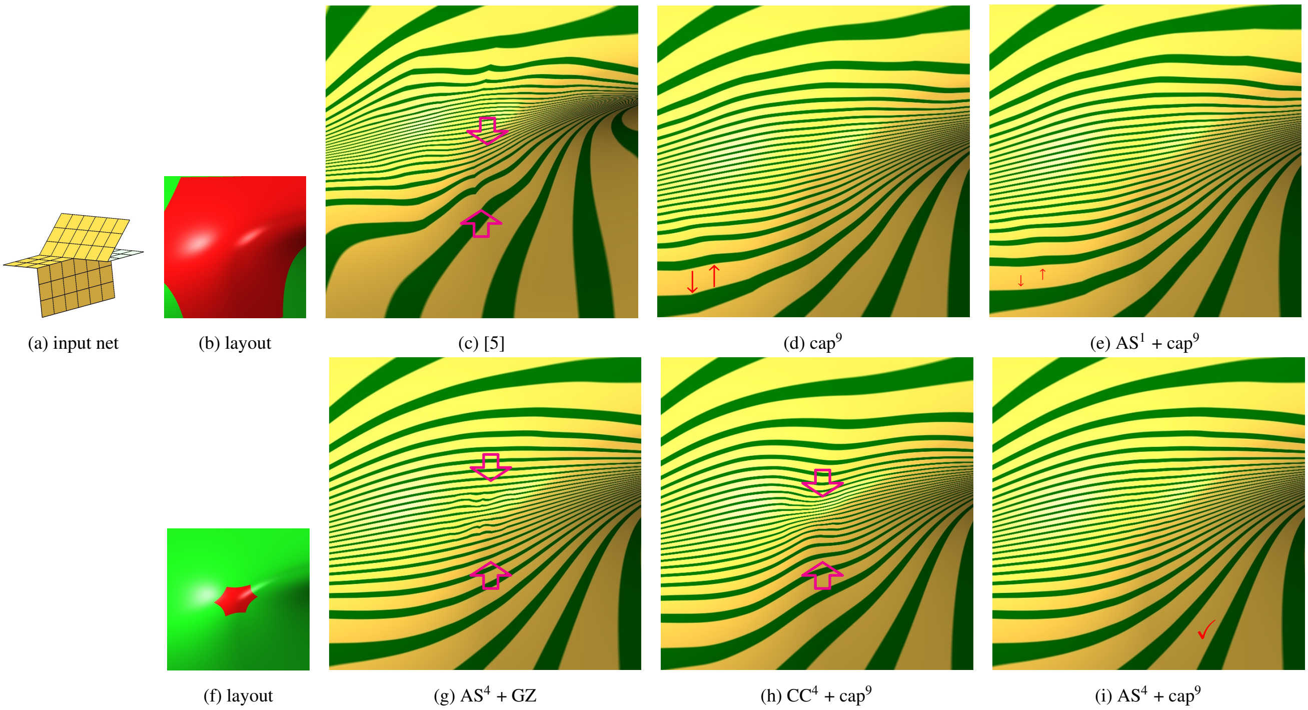

Figure 3: Bi-3 caps added after no or r subdivision steps. The number of surface rings r is indicated as superscript for CC^r [1] and AS^r [4]. The bi-cubic caps are: cap^9, the construction of Section 5.3; (c) [5], a 12 year old construction; (h) a cap construction GZ based on the constraints formulated 30 years ago in [6], see also Fig. 14 a. In (b,f) green indicates the surrounding regular bi-3 surface. Flaws are pointed to by ⇨, ↑ and ↓. (h) Combining the improved cap^9 with CC^4 leads to poor outcomes: the good cap cannot fix the structural problems of the underlying subdivision algorithm (the same is illustrated in Fig. 21 for [3]). (g) Conversely applying an old cap construction, here GZ, to a high-quality surrounding surface AS^4 fails to produce a good highlight line distribution. (d,e,i) Fewer visual oscillations when an improved subdivision, here AS^r, is completed with cap^9.

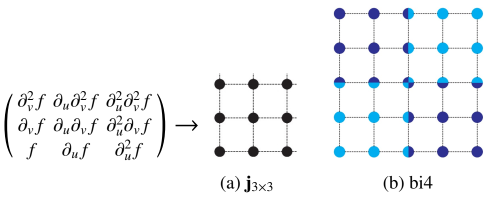

Figure 4: Corner jets and composing the bi-4 patches. (a) Partial derivatives at corner point are converted to BB-form of fixed degree bi-d; the BB-coefficients form BB-subnet $\mathbf{j}_{3\times3}$, called jet. (b) For $d = 4$ the four such $\mathbf{j}_{3\times3}$ are merged to form bi-4 patch by averaging the overlapping BB-coefficients. Restricting the construction to the two bottom rows in (a) and (b) shows how to combine jets $\mathbf{j}_{3\times2}$ at the corners to form a tensor-border of degree bi-4.

$\bar{\mathbf{t}}^0$ and $\bar{\mathbf{t}}^1$ are defined by BB-coefficients $\tilde{\mathbf{t}}^0_{ij}, \tilde{\mathbf{t}}^0_{3j}, \tilde{\mathbf{t}}^1_{3-ij}, i = 0, 1, j = 0, 1$ and the C^1 bi-4 tensor-border by

$$\begin{aligned}
\mathbf{t}_{00} &:= \bar{\mathbf{t}}^0_{00},\ \mathbf{t}_{10} := \frac{1}{2}(3\bar{\mathbf{t}}^0_{10} - \bar{\mathbf{t}}^0_{00}),\ \mathbf{t}_{20} := 2\bar{\mathbf{t}}^0_{30} - \frac{1}{2}(\bar{\mathbf{t}}^0_{10} + \bar{\mathbf{t}}^1_{20}),\\
\mathbf{t}_{01} &:= \frac{1}{2}(3\bar{\mathbf{t}}^0_{01} - \bar{\mathbf{t}}^0_{00}),\ \mathbf{t}_{11} := \frac{1}{4}(\bar{\mathbf{t}}^0_{00} - 3(\bar{\mathbf{t}}^0_{10} + \bar{\mathbf{t}}^0_{01}) + 9\bar{\mathbf{t}}^0_{11}), \qquad (1)\\
\mathbf{t}_{21} &:= 3\bar{\mathbf{t}}^0_{31} + \frac{1}{4}(\bar{\mathbf{t}}^0_{10} + \bar{\mathbf{t}}^1_{20} - 3(\bar{\mathbf{t}}^0_{11} + \bar{\mathbf{t}}^1_{21})) - \bar{\mathbf{t}}^0_{30}.
\end{aligned}$$

The remaining BB-coefficients $\mathbf{t}_{4-i,j}$, $i, j = 0, 1$ are obtained from $\mathbf{t}_{ij}$ by replacing $\bar{\mathbf{t}}^0_{ij}$ by $\bar{\mathbf{t}}^1_{3-i,j}$.

Tensor-borders $\mathbf{t}$ along the two outer boundary curves of one sector are joined to form L-shaped bi-4 tensor-borders, see Fig. 6 since they agree in their overlap data. Due to the shared Hermite data, the tensor-borders of neighboring sectors are C^2-connected. Removing the BB-coefficients shared by neighboring sectors yields truncated L-shaped tensor-borders whose coefficients are denoted by (see Fig. 6)

$$\mathbf{d}^s_{ij},\ s = 0, \ldots n-1. \qquad (2)$$

(These contain the full C^1 information since the removed BB-coefficients are defined as averages to enforce the C^1 join). Each sector s now retains 12 BB-coefficients that we index $\mathbf{d}^s_{ij}$ as shown on the left side of Fig. 6 for derivation. For implementation, it is more convenient to use the single-digit indexing of a vector, shown for the sector $s+1$ on the right side, i.e, $\mathbf{d}^{s+1}_k$, $k = 1, \ldots, 12$. The control points $\mathbf{d}^s$, $s = 0, \ldots, n-1$, and the point $\mathbf{c}_0$ derived from the subdivision algorithm form the input data for constructing the auxiliary bi-4 cap.

3.3. G^1 smoothness between adjacent sectors $\grave{\mathbf{p}}$ and $\acute{\mathbf{p}}$ and the use of target points $\grave{\mathbf{a}}_{i1}$ and $\acute{\mathbf{a}}_{i1}$

This section collates a number of technical facts for the derivation and a number of formulas for the concrete implementation of the algorithm. The polynomial pieces $\grave{\mathbf{p}}$ and $\acute{\mathbf{p}}$ of adjacent sectors (see Fig. 7 a) join G^1 along the common sector-separating curve $\grave{\mathbf{p}}(u, 0) = \acute{\mathbf{p}}(u, 0)$ with BB-coefficients $\grave{\mathbf{p}}_{i0} = \acute{\mathbf{p}}_{i0}$ if, see e.g. [31], after reparameterization $\grave{\mathbf{p}}(u, v) := \acute{\mathbf{p}} \circ \rho(u, v)$, $(u, v) \in [0..1]^2$,

$$\begin{aligned}
&\grave{\mathbf{p}} \sim \acute{\mathbf{p}} : \qquad (3)\\
&\partial_v \grave{\mathbf{p}} = a(u)\partial_v \acute{\mathbf{p}} + b(u)\partial_u \grave{\mathbf{p}}, \quad \rho(u, v) := (u + b(u)v, a(u)v).
\end{aligned}$$

By setting $a(u) := -1$ the sectors are treated symmetrically (without bias). Besides the shared BB-coefficients of common boundary, only the next layers $\grave{\mathbf{p}}_{i1}$ and $\acute{\mathbf{p}}_{i1}$ of adjacent patches enter the G^1 continuity constraints.

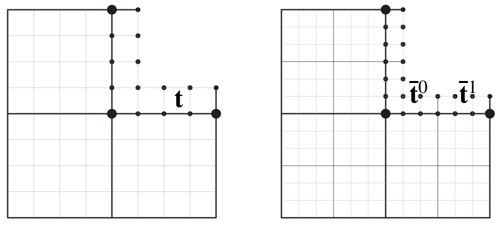

(a) single bi-4 (b) 2×2 bi-3

(c) $\{\bar{\mathbf t}^0, \bar{\mathbf t}^1\} \to \mathbf t$

Figure 5: Correspondence of tensor borders $\mathbf t$ (bi-4) and $\bar{\mathbf t}^0$, $\bar{\mathbf t}^1$ (bi-3): (a) Structure of the innermost ring of a C^2 bi-4 subdivision surface, say [2], and C^1 extension $\mathbf t$. (b) The innermost ring of a C^2 bi-3 subdivision surface, say [4] and C^1 extensions (tensor-borders) $\bar{\mathbf t}^0$ $\bar{\mathbf t}^1$. (c) Transformation of the C^2-connected bi-3 tensor-borders $\bar{\mathbf t}^0$ and $\bar{\mathbf t}^1$ to the bi-4 tensor-border $\mathbf t$.

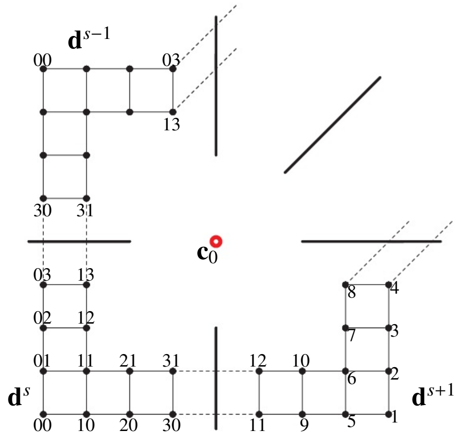

Figure 6: Input data $[\mathbf c_0, \mathbf d^s_{ij}]$ for constructing cap$^{\text{aux}}$: $12n$ control points partitioned into L-shaped sectors $\mathbf d^s$, $s = 0,\dots,n-1$, and a limit point $\mathbf c_0$ of the subdivision surface.

In this following, $b(u)$ is either the linear function $\mu(1-u)+\nu u$ or the quadratic function $\mu(1-u)^2$; in latter case, considering the caps of degree bi-d we assume that along the boundary $\grave{\mathbf p}|_{v=0}$ is of degree $d-1$. Hence in either case the function $b(u)\partial_u\grave{\mathbf p}$ is of degree d. Denoting its BB-coefficients $\mathbf e_i$, we get

$$\acute{\mathbf p}_{i1} := -\grave{\mathbf p}_{i1} + 2\grave{\mathbf p}_{i0} + \frac{1}{d}\mathbf e_i, \tag{4}$$

and write out, for linear $b(u)$,

$$\begin{aligned}
d = 3 &: [\mathbf e_2, \mathbf e_3] := [2\nu(\grave{\mathbf p}_{20} - \grave{\mathbf p}_{10}) + \mu(\grave{\mathbf p}_{30} - \grave{\mathbf p}_{20}), 3\nu(\grave{\mathbf p}_{30} - \grave{\mathbf p}_{20})];\\
d = 4 &: [\mathbf e_2, \mathbf e_3, \mathbf e_4] := [2\nu(\grave{\mathbf p}_{20} - \grave{\mathbf p}_{10}) + 2\mu(\grave{\mathbf p}_{30} - \grave{\mathbf p}_{20}),\\
&\qquad 3\mu(\grave{\mathbf p}_{30} - \grave{\mathbf p}_{20}) + \nu(\grave{\mathbf p}_{40} - \grave{\mathbf p}_{30}), 4\nu(\grave{\mathbf p}_{40} - \grave{\mathbf p}_{30})],
\end{aligned}$$

noting that $\mathbf e_i$, $i = 0, 1$ are obtained from $-\mathbf e_{d-k}$ by exchanging $\mu \leftrightarrow \nu$ and $\grave{\mathbf p}_{d-k,0} \leftrightarrow \grave{\mathbf p}_{k0}$, $k = 0, 1$. For quadratic $b(u) := \mu(1-u)^2$ we only need

$$d = 4: \quad \mathbf e_2 := \frac{2}{3}\mu(\grave{\mathbf p}_{40} - \grave{\mathbf p}_{30}).$$

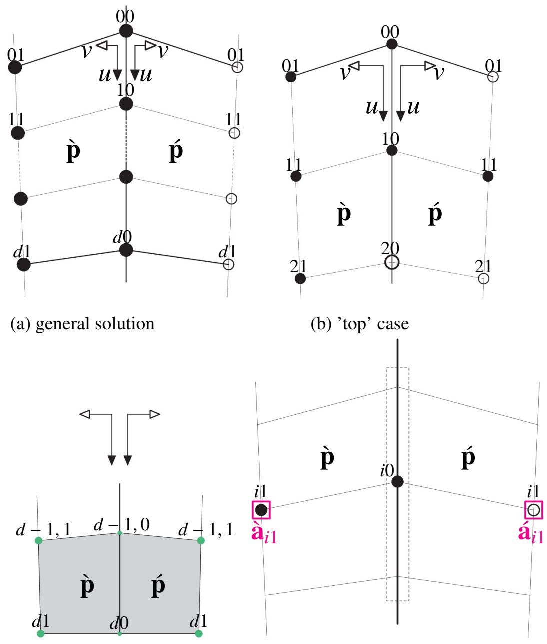

(a) general solution (b) 'top' case

(c) 'bottom' case (d) targets points $\square$

Figure 7: BB-subnets involved in the G^1-constraints between adjacent sectors. (a) General structure: solid arrows indicate parameterization by u, hollow ones by v. (b) BB-subnet attached to $\mathbf c_0$ ('top'), (c) BB-subnet adjacent to the innermost subdivision surface ring ('bottom'). (d) Guiding the cap by target points $\square$.

At the 'top', i.e. at the central point $\mathbf c_0 = \grave{\mathbf p}_{00}$, see Fig. 7 b, $b(u)$ is defined by $\mu := 2\mathsf c := 2\cos(2\pi/n)$ so (4) implies for $i = 0$ that $\acute{\mathbf p}_{01} := -\grave{\mathbf p}_{01} + 2\mathsf c\grave{\mathbf p}_{10} + 2(1-\mathsf c)\grave{\mathbf p}_{00}$. By recurrence, all $\grave{\mathbf p}^s_{01}$ and $\grave{\mathbf p}^s_{10}$ for $s > 0$ can be expressed in terms of $\grave{\mathbf p}^0_{01}$, $\grave{\mathbf p}^s_{10}$ and $\mathbf c_0$. This yields a well-defined tangent plane. When $i = 1$, we rearrange

$$\grave{\mathbf p}_{20} := \frac{1}{2\mathsf c(d-1)}\Big(\nu\grave{\mathbf p}_{00} + d(\grave{\mathbf p}_{11} + \acute{\mathbf p}_{11}) + 2(d\mathsf c - \mathsf c - d - \frac{\nu}{2})\grave{\mathbf p}_{10}\Big) \tag{5}$$

to treat BB-coefficients $\grave{\mathbf p}_{11}$ and $\acute{\mathbf p}_{11}$ as unconstrained (free). Therefore the circulant system of equations at $\mathbf c_0$ is satisfied and we can concentrate on local G^1-constraints between sectors.

At the 'bottom', connecting to the last subdivision ring r, see Fig. 7 c, we choose $b(u)$ either linear as $\mu(1-u)$ or quadratic as $\mu(1-u)^2$. In the linear case, $\mathbf e_d := 0$ and (4) implies $\grave{\mathbf p}_{d0} := \frac{1}{2}(\grave{\mathbf p}_{d1} + \acute{\mathbf p}_{d1})$. Since $\nu := 0$, in (4), a solution for $i = d-1$ is

$$\grave{\mathbf p}_{d-1,0} := \frac{1}{2d-\mu}\Big(d(\grave{\mathbf p}_{d-1,1} + \acute{\mathbf p}_{d-1,1}) - \mu\grave{\mathbf p}_{d0}\Big). \tag{6}$$

In the quadratic case $\mathbf e_{d-1} := 0 =: \mathbf e_d$; that is $\grave{\mathbf p}_{d-i,0} := \frac{1}{2}(\grave{\mathbf p}_{d-i,1} + \acute{\mathbf p}_{d-i,1})$ for $i = 0, 1$.

The 'middle' sections are under-constrained and are set to closely match target points $\grave{\mathbf a}_{i1}$ and $\acute{\mathbf a}_{i1}$, see Fig. 7 d. Minimizing $(\grave{\mathbf p}_{i1} - \grave{\mathbf a}_{i1})^2 + (\acute{\mathbf p}_{i1} - \acute{\mathbf a}_{i1})^2$ for the BB-coefficients $\grave{\mathbf p}_{i1}$ and $\acute{\mathbf p}_{i1}$ while enforcing (4) for fixed $\grave{\mathbf p}_{k0}$ yields the formula

$$\grave{\mathbf p}_{i1} := \frac{1}{2}(\grave{\mathbf a}_i - \acute{\mathbf a}_i) + \grave{\mathbf p}_{i0} + \frac{1}{2d}\mathbf e_i, \quad \acute{\mathbf p}_{i1} := \grave{\mathbf p}_{i1} - (\grave{\mathbf a}_i - \acute{\mathbf a}_i). \tag{7}$$

To apply the results local to two patches $\grave{\mathbf p}$ and $\acute{\mathbf p}$ to the n-sided cap, we set $\grave{\mathbf p} := \mathbf p^s$ and $\acute{\mathbf p} := \mathbf p^{s+1}$, $s = 0,\dots,n-1$. Fig. 8 a,b illustrates this re-labelling for the auxiliary bi-4 cap by juxtaposing local and global indices.

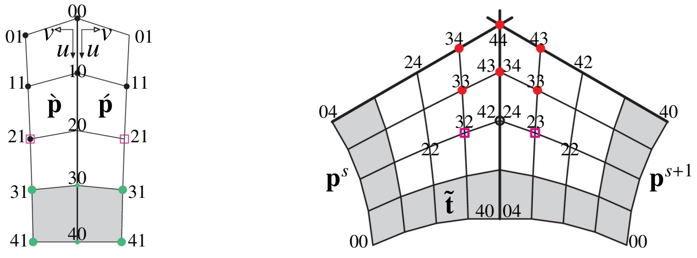

(a) G^1 constraints, local indexing (b) patch layout, global indexing

Figure 8: cap^{aux}: (a) local G^1 constraints; (b) structure of cap^{aux}.

4. Bi-4 caps

We now specialize the basic ideas of Section 3 to arrive at variants of bi-4 caps with different layout or formal smoothness properties. This section introduces cap^{aux} in Section 4.1 that encapsulates the shape of all subsequent caps of this paper, but meets the innermost surface ring of bi-4 subdivision only C^0. This section also defines $\text{cap}^{\boxplus}$ in Section 4.2 that achieves a C^1 connection to the innermost bi-4 subdivision ring at the cost of using a 2×2 macro-patch for each of the n sectors of the n-sided cap.

4.1. *The auxiliary bi-4 cap^{aux}*

The construction of the cap^{aux} is inspired by the bi-4 cap construction in [21]. The constructions differ since, in our setting, the input data are different: $\mathbf{d}^s$, $s = 0, \ldots, n-1$ of (2) and an undetermined central point $\mathbf{c}_0$. Following the framework of Section 3.3, Fig. 8 a shows the BB-subnets contributing to the G^1-constraints between sectors, with $b(u) := 2\mathsf{c}(1-u)$. B-coefficients, marked as black bullets in Fig. 8 a are unconstrained; $\grave{\mathbf{p}}_{20}$ is fixed by (5). Fig. 8 b shows the structure of cap^{aux}. Since C^1 smoothness of input tensor-border $\mathbf{t}$ is not consistent with (6), $\mathbf{t}$ is re-parameterized to $\mathbf{t} \circ \beta$ where

$$\begin{aligned} \beta(u,v) &:= (u, a(u)v), \qquad \mathsf{c} := \cos(2\pi/n), \\ a(u) &:= B_0^2(u) + B_1^2(u) + \frac{2}{2-\mathsf{c}} B_2^2(u). \end{aligned} \tag{8}$$

The BB-coefficients of the first-order expansion along the

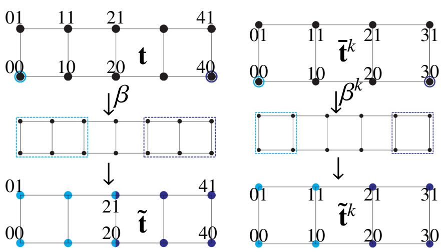

(a) bi-4 (b) bi-3

Figure 9: Transformation of input tensor-borders $\mathbf{t} \to \tilde{\mathbf{t}}$ and $\mathbf{t}^k \to \tilde{\mathbf{t}}^k$.

boundary curve form a tensor-border of degree 6, Fig. 9 a,*middle*. The 3×2 corner-jets, marked by cyan and blue dashed boxes, are expressed in bi-4 form and merged by averaging at overlapping locations. The result is the tensor-border $\tilde{\mathbf{t}}$ preserving the boundary: $\tilde{\mathbf{t}}_{i0} := \mathbf{t}_{i0}$, $i = 0, \ldots, 4$. Let $\dot{\mathbf{t}}_i := \mathbf{t}_{i1} - \mathbf{t}_{i0}$. Then

$$\begin{aligned} &\tilde{\mathbf{t}}_{01} := \mathbf{t}_{01},\ \tilde{\mathbf{t}}_{11} := \mathbf{t}_{11},\ \tilde{\mathbf{t}}_{21} := \mathbf{t}_{21} + \frac{\mathsf{c}(\dot{\mathbf{t}}_0 + 6\dot{\mathbf{t}}_2 - 8\dot{\mathbf{t}}_3 + 3\dot{\mathbf{t}}_4)}{12(2-\mathsf{c})}, \\ &\tilde{\mathbf{t}}_{31} := \mathbf{t}_{31} + \frac{\mathsf{c}(2\dot{\mathbf{t}}_3 - \dot{\mathbf{t}}_4)}{2(2-\mathsf{c})},\ \tilde{\mathbf{t}}_{41} := \mathbf{t}_{41} + \frac{\mathsf{c}\dot{\mathbf{t}}_4}{2-\mathsf{c}}\,. \end{aligned} \tag{9}$$

The tensor-border $\tilde{\mathbf{t}}$ (gray in Fig. 8) satisfies the G^1-constraints between sectors. As explained in Appendix 9.1, the remaining BB-coefficients of cap^{aux} are also affine weighted combinations of the input points $\mathbf{d}^s_{ij}$ and $\mathbf{c}_0$. Therefore the algorithm can be implemented by computing the BB-coefficients of the n bi-4 output patches by multiplying $[\mathbf{c}_0, \mathbf{d}^s]$ by the matrix that encapsulates the cap construction.

Algorithm cap^{aux}:
The bi-4 patch of each sector is obtained as follows, see Fig. 8 :

1. The input tensor-border $\mathbf{t}$ defines the gray underlaid BB-subnets in Fig. 8 a,b, i.e. $\mathbf{p}^s_{ij}$ for $i \in \{0, \ldots 4\}$, $j \in \{0, 1\}$ (and the diagonally symmetric ones) by (9).
2. Appendix Section 9.1 presents the formulas for $\mathbf{p}^s_{33}$ and $\mathbf{p}^s_{43}$. $\mathbf{p}^s_{42} := \grave{\mathbf{p}}_{20}$ is defined by (5) (note the switch to local indices).
3. With target points set by (17) formula (7) defines $\mathbf{p}^s_{32} := \acute{\mathbf{p}}_{21}$.
4. By symmetry, only $\mathbf{p}^s_{22}$ remains, and is defined by (18).

We summarize the properties of cap^{aux}.

Summary 1. *The outer boundary of cap^{aux} matches the last ring of bi-4 subdivision surface. cap^{aux} consists of n bi-4 patches that join G^1.*

4.2. *The C^1 bi-4 $\text{cap}^{\boxplus}$*

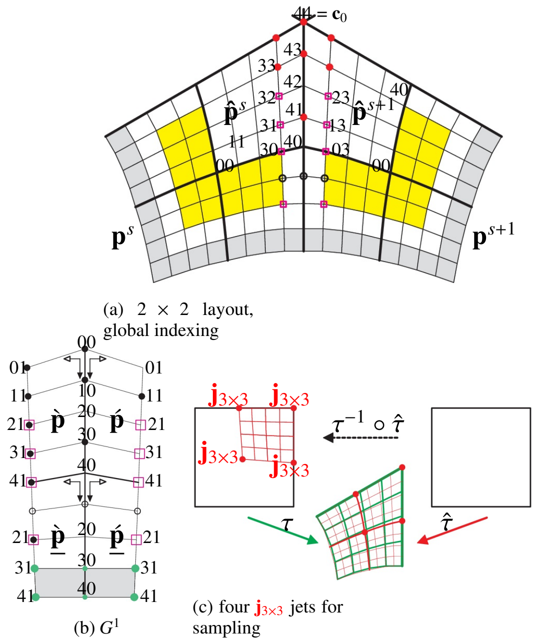

(a) 2×2 layout, global indexing

(b) G^1

(c) four $\mathbf{j}_{3\times3}$ jets for sampling

Figure 10: $\text{cap}^{\boxplus}$: (a) global structure. (b) G^1 constraints with local indices. (c) Constructing the 4 corner jets $\mathbf{j}_{3\times3}$ for sampling the central quadrant of cap^{aux}. In the *top,right* quadrant of the left square of (c), the 4 jets overlap in almost identical BB-coefficients and so, misleadingly, appear to form a bi-4 patch.

Quadrupling the number of patches to a 2×2 layout, see Fig. 10 a, the gray-underlaid BB-coefficients represent the input tensor-border $\mathbf{t}$, split into two. Therefore $\text{cap}^{\boxplus}$ is C^1-connected to the last bi-4 subdivision ring. We choose, see Fig. 10 b,

$$\text{top: } \grave{\mathbf{p}} \sim \acute{\mathbf{p}} \text{ with } b(u) := 2\mathsf{c}(1-u) + \frac{2}{3}\mathsf{c}u, \tag{10}$$

$$\text{bottom: } \underline{\grave{\mathbf{p}}} \sim \underline{\acute{\mathbf{p}}} \text{ with } \underline{b}(u) := \frac{2}{3}\mathsf{c}(1-u)^2, \quad \mathsf{c} := \cos(2\pi/n). \tag{11}$$

The BB-coefficients marked • are locally unconstrained (free) and $\color{green}\bullet$ coincide with the corresponding BB-coefficients of the split tensor-border $\mathbf{t}$.

The key to good shape is central bi-4 piece $\hat{\mathbf{p}}$ attached to $\mathbf{c}_0$. We compute the four $\mathbf{j}_{3\times3}$ corner jets of one sector at the corner points of $\tau^{-1}\circ\hat{\tau}$, where $\tau:\mathbb{R}^2\to\mathbb{R}^2$ is the planar cap$^{\mathrm{aux}}$ whose tensor-border $\mathbf{d}$ stems from the degree-raised characteristic map of Catmull-Clark subdivision and $\mathbf{c}_0$ coincides with the origin; $\hat{\tau}$ is taken from [28] adjusting for the input data, see Fig. 10 c. Then the center piece $\hat{\mathbf{p}}$ of cap$^{\boxplus}$is assembled, as illustrated in Fig. 4 , from cap$^{\mathrm{aux}}$ composed with each of the four 3×3 corner jets $\mathbf{j}_{3\times3}$. All BB-coefficients are affine combinations of the BB-coefficients of cap$^{\mathrm{aux}}$ and Appendix 9.2 lists all the derived weights explicitly to facilitate implementation.

Algorithm cap$^{\boxplus}$:
Each sector's BB-nets is obtained as, see Fig. 10 a,b:

1. The split input tensor-border $\mathbf{t}$ defines the gray underlaid BB-subnets in Fig. 10 a,b.
2. $\grave{\mathbf{p}}_{20}$ is calculated as (5) and
$$\grave{\mathbf{p}}_{40} := \frac{1}{17}\big(-6\grave{\mathbf{p}}_{20}+20\grave{\mathbf{p}}_{30}+4\underline{\grave{\mathbf{p}}}_{30}-\underline{\acute{\mathbf{p}}}_{40}\big)\,.$$
3. Set $\underline{\grave{\mathbf{p}}}_{00} := \grave{\mathbf{p}}_{40}$, $\underline{\grave{\mathbf{p}}}_{10} := 2\grave{\mathbf{p}}_{40}-\grave{\mathbf{p}}_{30}$, $\underline{\grave{\mathbf{p}}}_{20} := -\frac{1}{6}(\underline{\grave{\mathbf{p}}}_{00}+\underline{\grave{\mathbf{p}}}_{40})+\frac{2}{3}(\underline{\grave{\mathbf{p}}}_{10}+\underline{\grave{\mathbf{p}}}_{30})$. Then (7) defines $\grave{\mathbf{p}}_{i1}$ and $\acute{\mathbf{p}}_{i1}$, $i=2,3,4$.
4. The yellow-underlaid BB-subnet in Fig. 10 a is the C^2-extension of the central bi-4 piece. The BB-coefficients marked as $\color{magenta}\square$ serve as target points for defining $\underline{\grave{\mathbf{p}}}_{21}$ and $\underline{\acute{\mathbf{p}}}_{21}$ via formula (7).

We summarize the properties of cap$^{\boxplus}$.

Summary 2. *The outer boundary of cap$^{\boxplus}$ joins C^1 with the innermost bi-4 subdivision ring. Each sector of the n sectors of cap$^{\boxplus}$ consists of 2×2 C^1-joined bi-4 patches, and abutting sectors of cap$^{\boxplus}$ join G^1.*

5. Bi-3 caps

We derive three types of bi-3 caps. All three are internally smooth. $\widetilde{\mathrm{cap}}^{\boxplus}$ in Section 5.1 has the simplest layout, consisting of 2×2 patches per sector; as Section 7 clarifies $\widetilde{\mathrm{cap}}^{\boxplus}$ empirically has excellent highlight line distributions despite a slight normal discontinuity with the innermost bi-3 subdivision ring. A variant of $\widetilde{\mathrm{cap}}^{\boxplus}$ is introduced in Section 5.2: $\widetilde{\mathrm{cap}}^{9}$ features a novel 9-piece layout (but not a 3×3 split) of each sector, and reduces the normal mismatch still further. Section 5.3 derives cap^9 from cap$^{\boxplus}$: cap^9 guarantees a C^1-connection to the innermost bi-3 subdivision ring and introduces a different 9-piece layout. Since the bi-4 cap$^{\mathrm{aux}}$ is the starting point for all three bi-3 cap constructions to complete bi-3 subdivision surfaces, we transform the C^2-connected bi-3 tensor-borders $\tilde{\mathbf{t}}^0$ and $\tilde{\mathbf{t}}^1$ to a bi-4 tensor-border $\mathbf{t}$ as described in Section 3.2, Equation (1).

In the derivations we use two transformations T_1 and T_2 that map bi-4 patches to bi-3 patches, see Fig. 11 . T_1 maps a bi-4 patch to a single bi-3 patch preserving 2×2 corner-jets $\mathbf{j}_{2\times2}$ marked $\color{cyan}\square$ and $\color{blue}\square$ in Fig. 11 a in bi-4 form and merged to form the bi-3 patch. T_2 splits the bi-4 patch into 2×2 and retains the 3×3 corner jets $\mathbf{j}_{3\times3}$ with BB-coefficients $\color{cyan}\bullet$ and $\color{blue}\bullet$ in bi-3 form to define the corners of the 2×2 macro-patch that is completed by internal C^1 joining (that fortuitously turns out to be C^2), see Fig. 11 b.

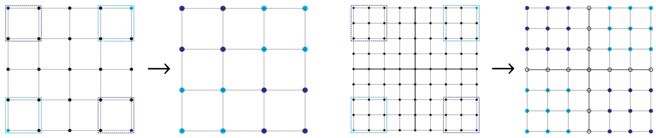

(a) T_1: bi-4 → bi-3 (b) T_2: bi-4 → 2×2 bi-3

Figure 11: Transformations T_1 and T_2.

5.1. *The almost smooth* $\widetilde{\mathrm{cap}}^{\boxplus}$

We transform cap$^{\mathrm{aux}}$ into a cap with 2×2 bi-3 pieces Fig. 12 b and apply T_2 to each piece. Choosing for G^1 constraints between sectors, see Fig. 12 a,

$$\text{top: } \grave{\mathbf{p}} \sim \acute{\mathbf{p}} \text{ with } b(u) := 2\mathsf{c}(1-u)+\mathsf{c}u, \tag{12}$$
$$\text{bottom: } \underline{\grave{\mathbf{p}}} \sim \underline{\acute{\mathbf{p}}} \text{ with } b(u) := \mathsf{c}(1-u), \qquad \mathsf{c} := \cos(2\pi/n) \tag{13}$$

yields the BB-coefficients of $\widetilde{\mathrm{cap}}^{\boxplus}$, marked in Fig. 12 b as $\color{red}\bullet$ and we retain $\color{green}\bullet$ in Fig. 12 a.

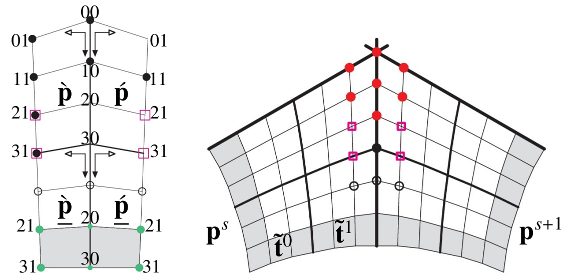

(a) G^1 (b) 2×2 layout

Figure 12: Almost smooth bi-3 $\widetilde{\mathrm{cap}}^{\boxplus}$. (a) G^1 constraints; (b) global structure.

We set $\grave{\mathbf{p}}_{30} := \grave{\mathbf{p}}_{20}+\frac{1}{4}(\underline{\grave{\mathbf{p}}}_{20}-\grave{\mathbf{p}}_{10})$, define $\grave{\mathbf{p}}_{i1}$ and $\acute{\mathbf{p}}_{i1}$, $i=2,3,$ by formula (7) with $\color{magenta}\square$ in Fig. 12 b as target points; and set those marked as ∘ by C^1-extension of $\grave{\mathbf{p}}$ and $\acute{\mathbf{p}}$.

The 2×2 bi-3 sectors are G^1-connected but need to be joined to the last subdivision ring. For

$$\beta^k(u,v) := (u, a^k(u)v), \tag{14}$$
$$a^0(u) := a(\frac{u}{2}),\ a^1(u) := a(\frac{1}{2}+\frac{u}{2}),$$

and a_0^k, a_1^k, a_2^k the BB-coefficients of $a^k(u)$, the transformations $h^k:\tilde{\mathbf{t}}^k\to\tilde{\mathbf{t}}^k$ of the bi-3 tensor-borders analogous to the bi-4 case are

$$\begin{aligned}
&\tilde{\mathbf{t}}_{i0}^k := \bar{\mathbf{t}}_{i0}^k, i=0,\dots,3, \qquad \dot{\mathbf{t}}_i^k := \bar{\mathbf{t}}_{i1}^k-\bar{\mathbf{t}}_{i0}^k,\\
&\tilde{\mathbf{t}}_{01}^k := \bar{\mathbf{t}}_{00}^k+a_0^k\dot{\mathbf{t}}_0^k,\ \tilde{\mathbf{t}}_{11}^k := \bar{\mathbf{t}}_{10}^k+\frac{2}{3}(a_1^k-a_0^k)\dot{\mathbf{t}}_0^k+a_0^k\dot{\mathbf{t}}_1^k,\\
&\tilde{\mathbf{t}}_{31}^k := \bar{\mathbf{t}}_{30}^k+a_2^k\dot{\mathbf{t}}_3^k,\ \tilde{\mathbf{t}}_{21}^k := \bar{\mathbf{t}}_{20}^k+\frac{2}{3}(a_1^k-a_2^k)\dot{\mathbf{t}}_3^k+a_2^k\dot{\mathbf{t}}_2^k\,.
\end{aligned} \tag{15}$$

The transformed tensor-borders $\tilde{\mathbf{t}}^k$ form the gray-underlaid BB-subnet in Fig. 12 b. G^1 continuity between the sectors is preserved since the transformation retained the BB-subnet underlaid-gray in Fig. 13 a.

Summary 3. *$\widetilde{\mathrm{cap}}^{\boxplus}$ consists of n sectors of 2×2 C^1-joined bi-3 patches. Abutting sectors join G^1. $\widetilde{\mathrm{cap}}^{\boxplus}$ is $C^{1-\epsilon}$-connected to the last subdivision ring.*

5.2. *The almost smooth* $\widetilde{\text{cap}}^9$

By increasing number of sector pieces to 9 and retaining internal smoothness and good shape, the small normal discrepancy to the last subdivision ring is further reduced as explained in Section 7.

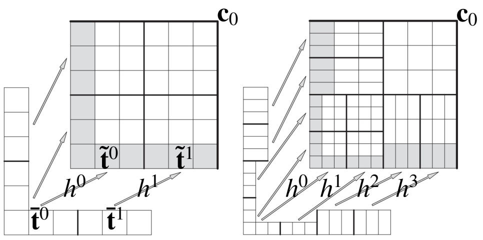

(a) 2×2 (b) 9 pieces

Figure 13: Transformations h^k for the $C^{1-\epsilon}$ $\widetilde{\text{cap}}^9$ construction.

In each sector all patches of $\widetilde{\text{cap}}^{\boxplus}$ see Fig. 13 a, except for the central piece, are uniformly split as displayed in Fig. 13 b: for two patches the split in one direction, for one patch in both directions. The correspondingly split tensor-borders are denoted $\bar{\mathbf{t}}^k$, $k = 0, 1, 2, 3$. Then $\widetilde{\text{cap}}^9$ is obtained replacing the gray-underlaid BB-coefficients by $h^k(\bar{\mathbf{t}}^k)$, $k = 0, 1, 2, 3$ where a^k_0, a^k_1, a^k_2 are the BB-coefficients of $a^k(u) := a(\frac{k}{4} + \frac{1}{4}u)$ and h^k the transformation defined by (15).

Summary 4. $\widetilde{\text{cap}}^9$ *consists of* n *sectors of 9* C^1*-joined bi-3 patches. Abutting sectors join* G^1 *and* $\widetilde{\text{cap}}^9$ *is* $C^{1-\epsilon}$*-connected to the last subdivision ring.*

5.3. *The smooth cap*^{9}

The $\widetilde{\text{cap}}^{\boxplus}$ and $\widetilde{\text{cap}}^9$ surfaces have good highlight line distributions. Here we investigate what price must be paid to enforce formal smoothness constraints, and this leads to a novel split into 9 patches, see Fig. 15 c.

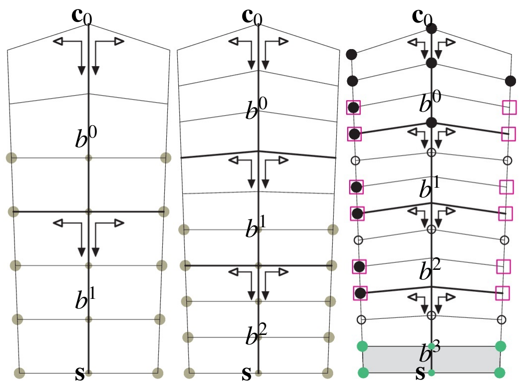

(a) [6] (b) [5] (c) cap^9

Figure 14: G^1 constraints with reparameterization b^k across the sector boundary $\mathbf{s}$ for smooth bi-3 caps.

We start with the observation that smooth transitions are not algebraically tricky: following [6], we can cover a sector with 2×2 macro-patches by choosing $b^0(u) := 2\mathtt{c}(1-u)^2$, $b^1(u) := 0$; that is, two thirds of the BB-net straddling the sector boundary $\mathbf{s}$ is parametrically C^1 connected, cf. the BB-coefficients marked $\circ$ in Fig. 14 a that are equidistant and opposite from the BB-coefficient on $\mathbf{s}$. [5] covers a sector with 3×3 patches and uses $b^0(u) := 2\mathtt{c}(1-u) + \mathtt{c}u$, $b^1(u) := \mathtt{c}(1-u)^2$, $b^2(u) := 0$ so that one half of the BB-net of two adjacent sectors is C^1 connected, cf. the BB-coefficients marked $\circ$ in Fig. 14 b. The challenge is the uniformity of highlight lines. Various experiments indicate that uniformity improves when strict C^1 constraints are pushed away from the central point $\mathbf{c}_0$. Therefore cap^9 uses four pieces along the sector boundary and $b^0(u) := 2\mathtt{c}(1-u) + \frac{4}{3}\mathtt{c}u$, $b^1(u) := \frac{4}{3}\mathtt{c}(1-u) + \frac{2}{3}\mathtt{c}u$, $b^2(u) := \frac{2}{3}\mathtt{c}(1-u) + \omega\mathtt{c}u$, $b^3(u) := \omega\mathtt{c}(1-u)^2$ which confines the strict C^1 pairs to those marked $\bullet$ in the gray underlaid BB-subnet. (The parameters $2\mathtt{c}$, $\frac{4}{3}\mathtt{c}$ and $\frac{2}{3}\mathtt{c}$ are inherited by subdivision from cap$^{\boxplus}$.) Further experiments indicate that setting ω close to the midpoint of interval $[\frac{1}{5}, \frac{1}{4}]$ as $\omega := \frac{1}{2}(\frac{1}{5} + \frac{1}{4}) = \frac{9}{40}$ yields empirically the best highlight lines. Denoting the BB-nets along $\mathbf{s}$ as $\grave{\mathbf{p}}^k$ and $\acute{\mathbf{p}}^k$, the BB-coefficients marked as $\circ$ are defined by C^1 extension of adjacent upper piece. The BB-coefficients marked $\bullet$ are for now unconstrained (free) and the BB-coefficients marked as $\bullet$ are obtained from the input tensor-border, $\grave{\mathbf{p}}^0_{20}$ is defined by (5). Once the BB-coefficients on $\mathbf{s}$ and the target points $\square$ have been decided upon, the BB-coefficients $\grave{\mathbf{p}}^k_{i1}$, $\acute{\mathbf{p}}^k_{i1}$, $i = 2, 3$, $k = 0, 1, 2$, follow from (7). In summary, the G^1 constraints hold for

$$
\begin{aligned}
\grave{\mathbf{p}}^1_{20} &:= \grave{\mathbf{p}}^0_{10} - 4\grave{\mathbf{p}}^0_{20} + 4\grave{\mathbf{p}}^0_{30},\\
\grave{\mathbf{p}}^1_{30} &:= \dot\omega_0\grave{\mathbf{p}}^0_{10} + \dot\omega_1\grave{\mathbf{p}}^0_{20} + \dot\omega_2\grave{\mathbf{p}}^0_{30} + \dot\omega_3\grave{\mathbf{p}}^3_{20} + \dot\omega_4\grave{\mathbf{p}}^3_{40},\\
\grave{\mathbf{p}}^2_{20} &:= \ddot\omega_1\grave{\mathbf{p}}^0_{10} + \ddot\omega_2\grave{\mathbf{p}}^0_{20} + \ddot\omega_3\grave{\mathbf{p}}^0_{30} + \ddot\omega_4\grave{\mathbf{p}}^1_{30},\\
\grave{\mathbf{p}}^2_{30} &:= \dddot\omega_1\grave{\mathbf{p}}^0_{10} + \dddot\omega_2\grave{\mathbf{p}}^0_{20} + \dddot\omega_3\grave{\mathbf{p}}^0_{30} + \dddot\omega_4\grave{\mathbf{p}}^1_{30} + \dddot\omega_5\grave{\mathbf{p}}^3_{20} + \dddot\omega_6\grave{\mathbf{p}}^3_{30},
\end{aligned}
$$

where

$$
\begin{aligned}
\underline{\omega} &:= \frac{1}{99\omega^2 - 414\omega + 32},\ \dot\omega_1 := -12\underline{\omega}(33\omega^2 - 147\omega + 10),\\
\dot\omega_2 &:= 4\underline{\omega}(99\omega^2 - 408\omega + 28),\ \dot\omega_3 := -6\underline{\omega}(23\omega - 2),\\
&\quad \dot\omega_4 := 2\underline{\omega}(33\omega - 2),\ \dot\omega_0 := 1 - \sum_{r=1}^{4}\dot\omega_r;\\
\ddot\omega_1 &:= \frac{3\omega - 16}{4},\ \ddot\omega_2 := 15 - 3\omega,\ \ddot\omega_3 := 1 - \ddot\omega_2,\ \ddot\omega_4 := -\ddot\omega_1;\\
\dddot\omega_1 &:= \frac{9}{20}\omega - \frac{12}{5},\ \dddot\omega_2 := 9 - \frac{9}{5}\omega,\ \dddot\omega_3 := \dddot\omega_2 + \frac{3}{5},\\
\dddot\omega_4 &:= -\dddot\omega_1,\ \dddot\omega_5 := \frac{3}{5},\ \dddot\omega_6 := -\frac{1}{5}\,.
\end{aligned}
$$

We now adjust the construction of cap$^{\boxplus}$ to bi-3 input replacing the gray-underlaid BB-net in Fig. 10 a by the input bi-3 tensor-borders degree-raised to degree bi-4. An intermediate collection of smoothly-joined bi-3 patches is constructed by applying T_1 to the central bi-4 piece and T_2 to the three others. Keeping the resulting BB-coefficients marked $\bullet$ or gray-underlaid in Fig. 15 a fixed, those marked $\square$ serve as target points in (7). Finally the BB-coefficients marked $\bullet$ are obtained by C^1 extension of the adjacent single bi-3 patch.

To reduce the number of patches per sector from 13 to 9 and improve the cap, the 4 pairs ℓ, r of bi-3 patches are merged and transformed to 4 bi-3 patches m in a following way, see Fig. 15 b: we set $\blacksquare := 2\diamond - 1\circ$; the $\circ$ remain fixed. This transformation preserves first order Hermite data along the boundaries defined by $\circ$. The yellow underlaid BB-coefficients are obtained by C^1 extension and a subsequent split of two m patches to restore internal smoothness of the sector.

Summary 5. *cap*^{9} *consists of* n *sectors of 9* C^1*-joined bi-3 patches. Abutting sectors join* G^1*. cap*^{9} *is* C^1*-connected to the last subdivision ring.*

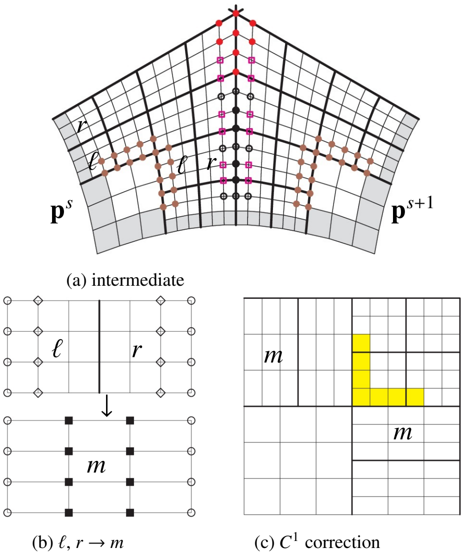

Figure 15: Construction of the smooth bi-3 cap^9 with 9 pieces per sector.

6. Gregory-type cap^G and polynomial counterpart cap$^{\text{bi5}}$

Gregory's approach [22] for combining inconsistent data was used in [32]. [33] generalized the approach to construct a smooth multi-sided surface by rationally averaging a series of interior BB-coefficients. cap^G uses this approach to combine the BB-coefficients $\mathbf{p}_{ij}$ of $\widetilde{\text{cap}}^{\boxplus}$ and $\mathbf{p}_{ij}$ of the input tensor-borders $\bar{\mathbf{t}}^0$, $\bar{\mathbf{t}}^1$. Fig. 16 a shows the cyan BB-net of $\widetilde{\text{cap}}^{\boxplus}$ and, in black, the tensor-border and $\circ$ of increasing size mark locations of inconsistency for one direction. Then setting

$$\circ_{01} := \frac{\mathbf{b}_{01}u^2 + \mathbf{p}_{01}v}{u^2+v}, \quad \circ_{11} := \frac{\mathbf{b}_{11}u^2 + \mathbf{p}_{11}v}{u^2+v},$$
$$\circ_{21} := \frac{\mathbf{b}_{21}(1-u)^2 + \mathbf{p}_{21}v}{(1-u)^2+v}, \quad \circ_{31} := \frac{\mathbf{b}_{31}(1-u)^2 + \mathbf{p}_{31}v}{(1-u)^2+v}\ .$$

yields C^1 2×2 macro patches per sector, that join G^1 to one another and C^1 to the last subdivision ring. (The diagonally symmetric rational BB-coefficients have $u \leftrightarrow v$ exchanged.)

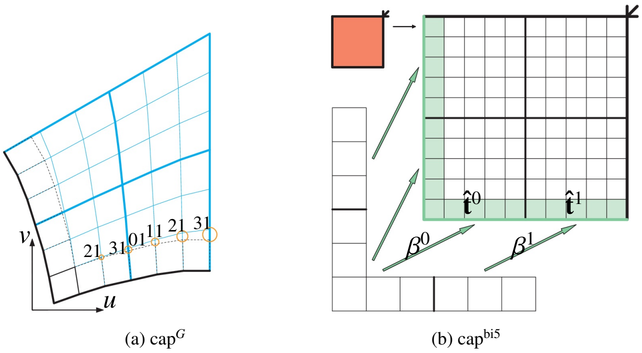

Figure 16: Sector of the smooth rational cap^G and its polynomial single piece per sector bi-5 alternative.

While Gregory's rational averaging reconciliates inconsistent data so that the resulting caps have reasonable shape, the implementation and conversion to rational BB-form is non-trivial: cap^G patches are rational of degree bi-7 and require special care at the corners where both numerator and denominator vanish. A more economic alternative, see Fig. 16 b, is to degree-raise cap$^{\text{aux}}$ to bi-5 and split the sectors into 2×2 pieces, reparameterize the input bi-3 tensor-borders as $\hat{\mathbf{t}}^k := \bar{\mathbf{t}}^k \circ \beta^k$ with the β^k of (14). See Appendix 9.3 for the construction of cap$^{\text{bi5}}$ illustrated in Fig. 9 b.

7. Interplay of smoothness, quality, degree and complexity

Referring back to the comparison of inter-sector constraints in Fig. 14 , we observe that simple construction can yield low degree bi-3, but at a noticeable cost to shape: the constraint pattern in Fig. 14 a from [6] yields simple, 2×2 per sector bi-3 surfaces that join the input ring C^1, but, as Fig. 3 g illustrates, yields a poor highlight line distribution.

The construction [19], with its 2×2 sector layout of degree bi-4 pieces, requires structure adjustment via a transition ring, namely to match the subdivision rings and reduce the inter-sector constraints to the structure in Fig. 14 a, in degree bi-4 form. The analysis of Fig. 20 indicates that such a transition already by itself harms the shape of high-quality subdivision. To be sure that the structural transition causes shape problems, we also extended the GZ construction (cf. Fig. 3 g) to degree bi-4, denoted GZ4 below. Fig. 17 illustrates the resulting poor surface quality.

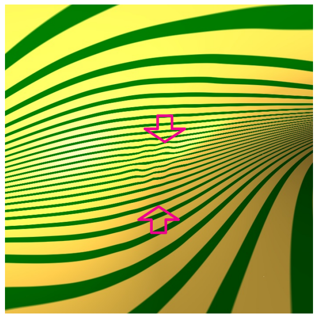

Figure 17: GZ4 capping AS^4 with input Fig. 3 a.

Increasing the complexity of the reparameterization to yield the constraint pattern of Fig. 14 b fails to improve highlight lines substantially, see Fig. 3 c (a slightly unfair comparison, due to not having applied any subdivision steps, but still indicative). The discussion of Fig. 20 shows that adding a transition ring to accommodate the data also fails. Only the more complex constraint pattern of Fig. 14 c, used by cap^9 and hidden in its pre-calculated formulas, leads to formal smoothness and good quality for degree bi-3. Increasing the degree to bi-4, cap$^{\boxplus}$ also yields uniform highlight lines and has the additional advantage that these bi-4 surfaces are G^1-refinable whereas bi-3 caps can not be G^1-refinable [28]. Another option to design the high quality multi-sided bi-3 internally smooth caps with 2×2 patches per sector comes at the cost of mismatch of normals on the boundary. In [20] a maximal normal mismatch of $< 0.1^o$ was reported, sufficient for automobile class A surfaces. We call this $C^{1-\epsilon}$ continuity. Initial subdivision steps reduce the mismatch below relevance for most applications.

For a convex net and $n = 8$, Fig. 18 compares capping AS^6, including with GZ4. The highlight lines of cap$^{\text{bi5}}$ are on par with $\widetilde{\text{cap}}^{\boxplus}$ and cap$^{\boxplus}$; cap^9 has slight oscillations at the transition to the last AS^6 ring, and these are more accentuated for cap^G, partly because the BB-coefficients averaged differ more than for the low valencies. From afar, both cap$^{\text{bi5}}$ and GZ4 surfaces look good, but the drastic difference in the highlight lines under zoom demonstrates the influence of the reparameterizations even in a small area after many refinement steps.

Fig. 19 juxtaposes the caps after step 2 (left column) and 6 (right column) of bi-3 AS subdivision, corresponding to minimally, respectively maximally many steps in practice. The normal mismatch for $\widetilde{\text{cap}}^{\boxplus}$ is $< 0.1^o$ in all tested cases and the highlight line distribution is on par with the strictly smooth cap$^{\boxplus}$. The highlight lines of $\widetilde{\text{cap}}^9$ are also visually indistinguishable

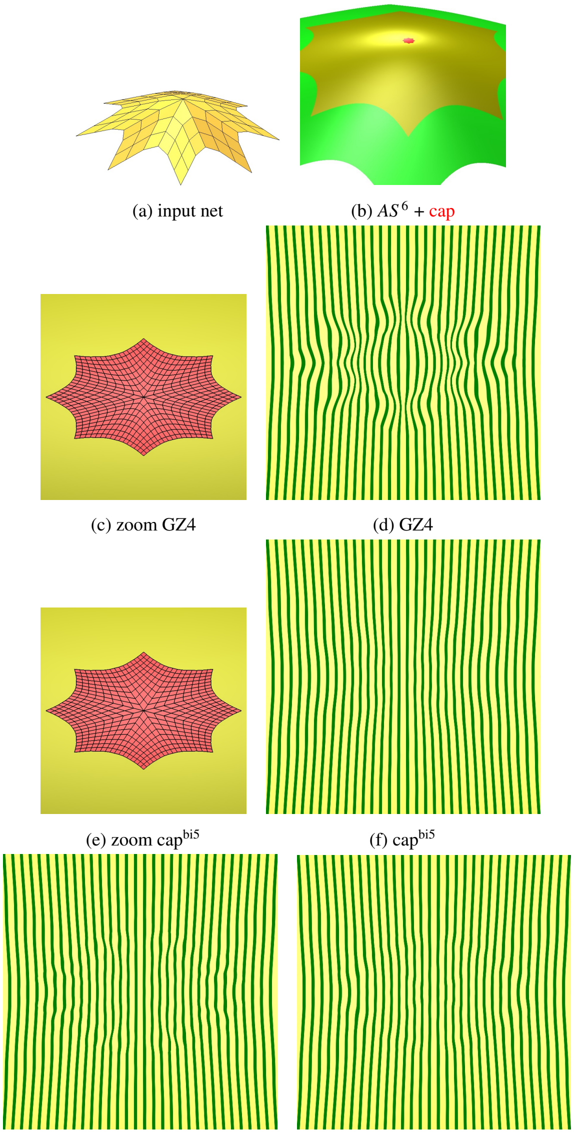
(a) input net (b) AS^6 + cap
(c) zoom GZ4 (d) GZ4
(e) zoom cap^{bi5} (f) cap^{bi5}
(g) cap^{G} (h) cap^{9}

Figure 18: Comparison of caps under zoom via highlight lines. (b) bi-3 surrounding surface, AS^6 subdivision rings (gold) and cap.

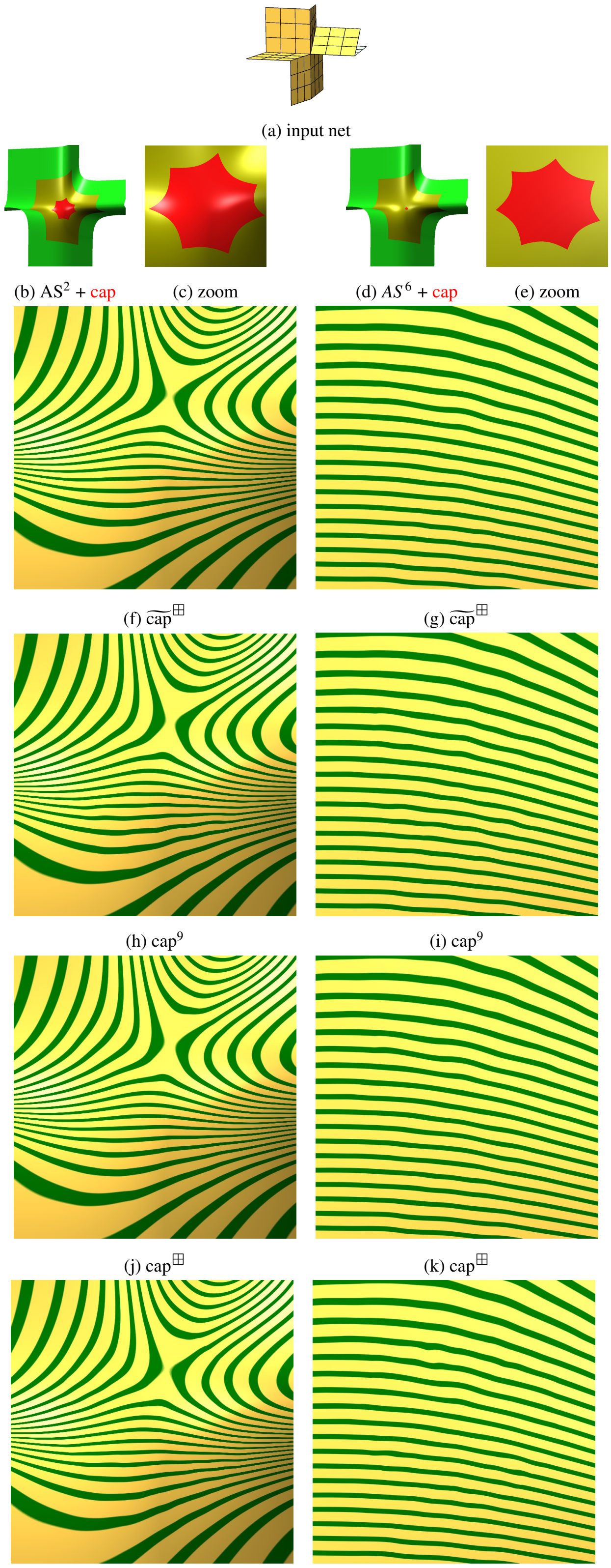
(a) input net
(b) AS^2 + cap (c) zoom (d) AS^6 + cap (e) zoom
(f) $\widetilde{\text{cap}}^{\boxplus}$ (g) $\widetilde{\text{cap}}^{\boxplus}$
(h) cap^{9} (i) cap^{9}
(j) $\text{cap}^{\boxplus}$ (k) $\text{cap}^{\boxplus}$
(l) cap^{G} (m) cap^{G}

Figure 19: Cap comparison: bi-cubic caps and cap^G. The zoom region for the left column is shown in (c) for the right in (e).

from those of $\widetilde{\text{cap}}^{\boxplus}$, but the normal mismatch for $\widetilde{\text{cap}}^{9}$ after AS^6 is $< 0,0081^o$. While this is formally $C^{1-\epsilon}$, the mismatch is less than 8 digits after the decimal point ($\arccos(0.99999999) \approx 0.0081028^o$), a level of accuracy acceptable in most modeling packages. For AS^2, the highlight lines of $\widetilde{\text{cap}}^{\boxplus}$ and $\text{cap}^{\boxplus}$ barely differ; cap^9 exhibits waviness, milder for cap^G. Under zoom, after AS^6, cap^9 exhibits fainter waves than cap^G.

Fig. 20 explores how even high-end surface constructions fail to produce a good cap for high-end subdivision due to the need to transition to their input data. Focusing on roughly the same surface region from the center as in Fig. 19 e, Fig. 20 a shows the cap of [7] applied after six steps of AS via a cyan bi-3 transition ring: the cap joins G^1 with the transition and is internally G^1 consisting of 2×2 bi-4 sectors; Fig. 20 b shows unexpected highlight line oscillations. Fig. 20 c,d show similar noise introduced, by inserting just the transition and then switching back to the original high-quality subdivision AS' rather than continuing throughout with AS steps as in Fig. 20 e.

Fig. 21 illustrates that even the new caps cannot fix the struc-

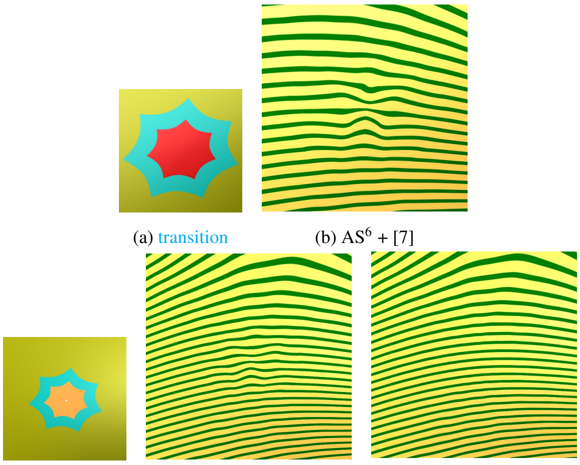

(a) transition (b) AS^6 + [7]

(c) transition (d) AS^6 + cyan + AS^6 (e) AS^{13} + $cap^{\boxplus}$

Figure 20: How transitions to accommodate the ring structure rule out otherwise high-end caps, here [7] and AS^r.

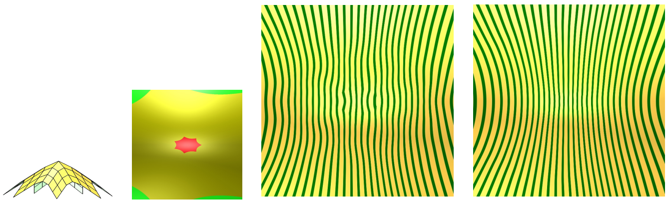

(a) $n = 7$ (b) layout (c) $[3]^4$ + $cap^{\boxplus}$ (d) AS^4 + $cap^{\boxplus}$

Figure 21: High-quality caps require high-quality subdivision.

tural problems introduced by lower quality subdivision with the AS layout, e.g. [3].

Limitations While higher-degree, more complex caps can be applied without subdivision, taking into account second-order Hermite data, we focused here on the covering simpler, low degree options that assume that the input data stem from a high-quality bi-3 or bi-4 subdivision scheme after $r > 1$ subdivision steps. These subdivision schemes smooth the features of the initial control net so that highlight lines vary smoothly although only first-order Hermite data is captured at the transition to the cap.

Adjusting to subdivision algorithms that generate $k \times k$ macro-patches for each of the three pieces of an L-shape is possible. We restricted any detailed treatment to the most common subdivision schemes that feature at most a 2×2 split.

8. Conclusion

The preceding sections exposed and compared alternatives for smoothly filling, with caps of degree bi-3 or bi-4, the multi-sided hole left in a surface after generating a fixed number of bi-3 or bi-4 subdivision rings. While a number of solutions exist in the literature, the recent introduction of improved subdivision algorithms reveals their comparatively poor shape characteristics. The gamut of the new bi-3 or bi-4 caps trades formal enforcement of algebraic mathematical smoothness constraints for good shape inherited from a control net and improved subdivision. The exhaustive overview of choices comes with explicit formulas for implementation.

References

[1] E. Catmull, J. Clark, Recursively generated B-spline surfaces on arbitrary topological meshes, Computer-Aided Design 10 (1978) 350–355.
[2] K. Karčiauskas, J. Peters, Evolving guide subdivision, Computer Graphics Forum (to appear) 1–12.
[3] Y. Ma, W. Ma, Subdivision schemes with optimal bounded curvature near extraordinary vertices, Computer Graphics Forum 37 (7) (2018) 455–467.
[4] K. Karčiauskas, J. Peters, Point-augmented bi-cubic subdivision surfaces, in: N. Umetani, E. Vouga, C. Wojtan (Eds.), Pacific Graphics 2022, The Eurographics Association and John Wiley & Sons Ltd., pp. 1–11.
[5] J. Fan, J. Peters, Smooth bi-3 spline surfaces with fewest knots, Computer Aided Design 43 (2) (2011) 180–187, jCAD 1686.
[6] J. A. Gregory, J. Zhou, Filling polygonal holes with bicubic patches, Computer Aided Geometric Design 11 (4) (1994) 391–410, iSSN 0167-8396.
[7] K. Karčiauskas, T. Nguyen, J. Peters, Generalizing bicubic splines for modeling and IGA with irregular layout, Computer-Aided Design 70 (2016) 23–35.
[8] K.-P. Beier, Y. Chen, Highlight-line algorithm for realtime surface-quality assessment, Comp-Aid Design 26 (4) (1994) 268–277.
[9] C. T. Loop, S. Schaefer, G^2 tensor product splines over extraordinary vertices, Comput. Graph. Forum 27 (5) (2008) 1373–1382.
[10] K. Karčiauskas, J. Peters, Minimal bi-6 G^2 completion of bicubic spline surfaces, Computer Aided Geometric Design 41 (2016) 10–22.
[11] G. J. Hettinga, J. Kosinka, A multisided C^2 B-spline patch over extraordinary vertices in quadrilateral meshes, Computer-Aided Design 127 (2020) 102855.
[12] M. Vaitkus, T. Várady, P. Salvi, Á. Sipos, Multi-sided b-spline surfaces over curved, multi-connected domains, Computer Aided Geometric Design 89 (2021) 102019.
[13] M. A. Sabin, C. Fellows, J. Kosinka, Cad model details via curved knot lines and truncated powers, Computer-Aided Design 143 (2022) 103137.
[14] X. Gu, Y. He, H. Qin, Manifold splines, in: Proceedings of the 2005 ACM symposium on Solid and physical modeling, 2005, pp. 27–38.
[15] M. Kapl, G. Sangalli, T. Takacs, Dimension and basis construction for analysis-suitable G^1 two-patch parameterizations, Computer Aided Geometric Design 52-53 (2017) 75–89.
[16] A. Blidia, B. Mourrain, G. Xu, Geometrically smooth spline bases for data fitting and simulation, Computer Aided Geometric Design 78 (2020) 101814.
[17] M. Marsala, A. Mantzaflaris, B. Mourrain, G1-smooth biquintic approximation of Catmull-Clark subdivision surfaces, Computer Aided Geometric Design 99 (2022) 102158.
[18] K. Karčiauskas, J. Peters, Improved shape for multi-surface blends, Graphical Models 82 (2015) 87–98.
[19] G.-P. Bonneau, S. Hahmann, Flexible G^1 interpolation of quad meshes, Graphical Models 76 (6) (2014) 669–681.
[20] K. Karčiauskas, J. Peters, Can bi-cubic surfaces be class A?, Computer Graphics Forum 34 (5) (2015) 229–238.
[21] K. Karčiauskas, J. Peters, Bi-cubic scaffold surfaces (2022) 1–10.
[22] J. A. Gregory, Smooth interpolation without twist constraints, Academic Press, 1974, pp. 71–88.
[23] C. T. Loop, S. Schaefer, T. Ni, I. Castaño, Approximating subdivision surfaces with Gregory patches for hardware tessellation, ACM Trans. Graph 28 (5) (2009) 151:1–151:9.
[24] P. Salvi, T. Várady, Multi-sided surfaces with fullness control, in: Proceedings of the Eighth Hungarian Conference on Computer Graphics and Geometry, 2016, pp. 61–69.
[25] K. Karčiauskas, J. Peters, A new class of guided C^2 subdivision surfaces combining good shape with nested refinement, in: Computer Graphics Forum, Vol. 37, Wiley Online Library, 2018, pp. 84–95.
[26] C. Gonzalez-Ochoa, S. McCammon, J. Peters, Computing moments of objects enclosed by piecewise polynomial surfaces, ACM Transactions on Graphics (TOG) 17 (3) (1998) 143–157.
[27] X. Wei, X. Li, Y. J. Zhang, T. J. Hughes, Tuned hybrid nonuniform subdivision surfaces with optimal convergence rates, International Journal for Numerical Methods in Engineering 122 (9) (2021) 2117–2144.
[28] K. Karčiauskas, J. Peters, Least degree G^1-refinable multi-sided surfaces suitable for inclusion into C^1 bi-2 splines, Computer-Aided Design 130 (2021) 1–12.
[29] C. de Boor, B-form basics, in: G. Farin (Ed.), Geometric Modeling: Algorithms and New Trends, SIAM, 1987, pp. 131–148.
[30] G. Farin, Curves and Surfaces for Computer Aided Geometric Design: A Practical Guide, Academic Press, 1988.

[31] T. D. DeRose, Necessary and sufficient conditions for tangent plane continuity of Bézier surfaces, Comp Aid Geom Design 7 (1) (1990) 165–179.
[32] C. Loop, S. Schaefer, T. Ni, I. Castano, Approximating subdivision surfaces with Gregory patches for hardware tessellation, in: ACM SIGGRAPH Asia 2009 papers, 2009, pp. 1–9.
[33] K. Karčiauskas, J. Peters, Localized G-splines for quad & T-gon meshes, in: Y. L. T Ju, J Kosinka (Ed.), Proc of GMP 2019, 2019, pp. 1–10.

9. Appendix

This Appendix contains the remaining technical formulas for the implementation of cap$^{\text{aux}}$, cap$^{\boxplus}$ and cap$^{\text{bi5}}$. For $n = 6$, the formulas and their use of tables A are illustrated in Section 9.1 and for K in Section 9.2. The tables for $n = 3, 5, 7, 8, 9, 10$ follow in Section 9.4 and Section 9.5. Section 9.3 lists the key formulas for cap$^{\text{bi5}}$.

9.1. *Tables and assignments of cap^{aux}*

Labeling the sectors of cap$^{\text{aux}}$

$$s = 0, \dots, n-1, \qquad \text{we set } \mathbf{p}^s_{44} := \mathbf{c}_0,$$

$$\mathbf{p}^s_{33} := \dot{a}_0 \mathbf{c}_0 + \sum_{r=0}^{n-1} \sum_{k=1}^{12} \dot{a}^r_k \mathbf{d}^{s+r}_k; \ \tilde{\mathbf{p}}^s_{43} := \ddot{a}_0 \mathbf{c}_0 + \sum_{r=0}^{n-1} \sum_{k=1}^{12} \ddot{a}^r_k \mathbf{d}^{s+r}_k, \quad (16)$$

$$\dot{a}_0 := 1 - \sum_{r=0}^{n-1} \sum_{k=1}^{12} \dot{a}^r_k, \ \ddot{a}_0 := 1 - \sum_{r=0}^{n-1} \sum_{k=1}^{12} \ddot{a}^r_k.$$

One choice for $\mathbf{c}_0$ is the modified Catmull-Clark limit point of [21]. For an efficient tabulation, due to rotational symmetry of the construction, it suffices to store only $\mathbf{p}^0_{33}$ and $\tilde{\mathbf{p}}^0_{43}$. Without sacrificing quality, $\dot{a}^r_k$ and $\ddot{a}^r_k$ need only be stored up to 5 digits after the decimal point precalculated as tables A^n_{33} and A^n_{43} of size $n \times 12$, for valences $n = 3, 5, \dots, 10$:

$$\dot{a}^r_k := \frac{1}{10^5} (A^n_{33})_{r+1,k}, \ \ \ddot{a}^r_k := \frac{1}{10^5} (A^n_{43})_{r+1,k}, \quad r = 0, \dots, n-1.$$

For example, for $n = 6$

$$A^6_{33} := \begin{pmatrix} 1436 & 1266 & -941 & -12151 & 1266 & -16291 & 7231 & 28028 & -941 & 7231 & -12151 & 28028 \\ 277 & -781 & -37 & -1546 & 2015 & -5212 & 7211 & -685 & -35 & -2622 & -5284 & 14625 \\ -588 & -712 & 93 & 4226 & -398 & 6127 & -1523 & -10354 & 546 & -2833 & 5314 & -11427 \\ -295 & -1078 & -228 & 4221 & -1078 & 6388 & -1714 & -7693 & -228 & -1714 & 4221 & -7693 \\ -588 & -398 & 546 & 5314 & -712 & 6127 & -2833 & -11427 & 93 & -1523 & 4226 & -10354 \\ 277 & 2015 & -35 & -5284 & -781 & -5212 & -2622 & 14625 & -37 & 7211 & -1546 & -685 \end{pmatrix},$$

$$A^6_{43} := \begin{pmatrix} 472 & 922 & -153 & -4706 & 356 & -6185 & 1426 & 11036 & -235 & 3453 & -4224 & 8448 \\ 472 & 356 & -235 & -4224 & 922 & -6185 & 3453 & 8448 & -153 & 1426 & -4706 & 11036 \\ 0 & -565 & -82 & 481 & 565 & 0 & 2026 & -2588 & 82 & -2026 & -481 & 2588 \\ -472 & -922 & 153 & 4706 & -356 & 6185 & -1426 & -11036 & 235 & -3453 & 4224 & -8448 \\ -472 & -356 & 235 & 4224 & -922 & 6185 & -3453 & -8448 & 153 & -1426 & 4706 & -11036 \\ 0 & 565 & 82 & -481 & -565 & 0 & -2026 & 2588 & -82 & 2026 & 481 & -2588 \end{pmatrix},$$

Tables A^n_{ij} for other valencies n are listed in Section 9.4. To ensure smoothness at the central point $\mathbf{c}_0$ after the 5 digit truncation, we recompute

$$\mathbf{p}^s_{43} := \mathbf{c}_0 + \frac{2}{n} \sum_{j=0}^{n-1} \cos(\frac{2\pi}{n} j) \tilde{\mathbf{p}}^{s+j}_{43},$$

calculate the gray-underlaid BB-coefficients in Fig. 8 by Equation (9) and set the target points as

$$\grave{\mathbf{a}}_{21} := \frac{2}{3}(\grave{\mathbf{p}}_{31} + \grave{\mathbf{p}}_{11}) - \frac{1}{6}(\grave{\mathbf{p}}_{41} + \grave{\mathbf{p}}_{01}) \qquad (17)$$

and $\acute{\mathbf{a}}_{21}$ analogously. Then $\grave{\mathbf{p}}_{20}$ follows from (5), $\grave{\mathbf{p}}_{21}$ and $\acute{\mathbf{p}}_{21}$ from (7) and

$$\mathbf{p}^s_{22} := \frac{1}{2}\Big(\frac{2}{3}(\mathbf{p}^s_{21} + \mathbf{p}^s_{23}) - \frac{1}{6}(\mathbf{p}^s_{20} + \mathbf{p}^s_{24})\Big) + \qquad (18)$$
$$\frac{1}{2}\Big(\frac{2}{3}(\mathbf{p}^s_{12} + \mathbf{p}^s_{32}) - \frac{1}{6}(\mathbf{p}^s_{02} + \mathbf{p}^s_{42})\Big).$$

9.2. *Tables and assignments of cap$^{\boxplus}$*

We define the BB-net $\hat{\mathbf{p}}_{rs}$ of the central piece attached to $\mathbf{c}_0$ in terms of the BB-coefficients $\mathbf{p}_{ij}$ of cap$^{\text{aux}}$ and tabulated κ^{rs}_{ij} as

$$\hat{\mathbf{p}}_{rs} := \sum_{i=0}^{4} \sum_{j=0}^{4} \kappa^{rs}_{ij} \mathbf{p}_{ij}, \quad 0 \le r, s \le 2,$$

$$\kappa^{rs}_{ij} := \frac{1}{10^5} (K^n_{rs})_{i+1,j+1}, \quad rs \in \{00, 10, 20, 11, 21, 22\},$$

$\kappa^{rs}_{ij} := \kappa^{sr}_{ji}$ for $(rs) \in \{01, 02, 12\}$ by symmetry and we need not superscript $\hat{\mathbf{p}}_{rs}$ since all formulas are the same for each sector. The 5 digits-after-decimal-point weights κ^{rs}_{ij}, scaled by 10^5, are recorded in tables K^n_{ij} (whose size does not depend on the valence n) of size 5×5 for $ij \in \{00, 10, 20, 11, 21, 22\}$, size 4×10 for K^n_3 and 1×5 for $ij \in \{41, 43\}$:

$$K^6_{00} := \begin{pmatrix} 520 & 1935 & 2698 & 1672 & 388 \\ 1935 & 7195 & 10032 & 6216 & 1444 \\ 2698 & 10032 & 13987 & 8667 & 2014 \\ 1672 & 6216 & 8667 & 5371 & 1248 \\ 388 & 1444 & 2014 & 1248 & 299 \end{pmatrix}, K^6_{10} := \begin{pmatrix} 48 & 1156 & 2971 & 2684 & 819 \\ 115 & 4057 & 10713 & 9772 & 2998 \\ 71 & 5320 & 14468 & 13334 & 4113 \\ -11 & 3088 & 8675 & 8082 & 2507 \\ -15 & 669 & 1948 & 1836 & 582 \end{pmatrix},$$

$$K^6_{20} := \begin{pmatrix} -12 & 77 & 2508 & 3928 & 1745 \\ -37 & 163 & 8276 & 13945 & 6267 \\ -34 & 69 & 10216 & 18456 & 8439 \\ -7 & 2 & -29 & 1142 & 2360 \end{pmatrix}, K^6_{11} := \begin{pmatrix} 17 & 122 & 158 & 34 & -20 \\ 122 & 2501 & 6001 & 5066 & 1441 \\ 158 & 6001 & 15442 & 13660 & 4056 \\ 34 & 5066 & 13660 & 12370 & 3739 \\ -20 & 1441 & 4056 & 3739 & 1156 \end{pmatrix},$$

$$K^6_{21} := \begin{pmatrix} -3 & 28 & 276 & 252 & -110 \\ -34 & 181 & 5196 & 7798 & 2994 \\ -57 & 200 & 11712 & 19522 & 8520 \\ -26 & 5 & 9310 & 16842 & 7743 \\ 0 & -42 & 2498 & 4869 & 2326 \end{pmatrix}, K^6_{22} := \begin{pmatrix} 520 & 1935 & 2698 & 1672 & 388 \\ 1935 & 7195 & 10032 & 6216 & 1444 \\ 2698 & 10032 & 13987 & 8667 & 2014 \\ 1672 & 6216 & 8667 & 5371 & 1248 \\ 388 & 1444 & 2014 & 1248 & 299 \end{pmatrix}.$$

$$K^6_3 := \begin{pmatrix} 4971 & 16014 & 19346 & 10387 & 2091 & 3897 & 13537 & 17542 & 10056 & 2159 \\ 474 & 9864 & 21987 & 17212 & 4554 & 224 & 7434 & 18325 & 15519 & 4407 \\ -198 & 572 & 18471 & 26871 & 9912 & -131 & 162 & 13444 & 21737 & 9160 \\ 0 & 0 & 0 & 32641 & 24048 & 0 & 0 & 0 & 24048 & 19263 \end{pmatrix},$$

$$K^6_{41} := \begin{pmatrix} 669 & 17942 & 40744 & 32115 & 8530 \end{pmatrix}, K^6_{43} := \begin{pmatrix} 0 & 0 & 0 & 57133 & 42867 \end{pmatrix}.$$

The tables K^n for $n \neq 6$ are listed in Section 9.5. Then

$$\hat{\mathbf{p}}_{44} := \mathbf{p}_{44}, \ \hat{L}_3 := \frac{1}{10^5} K^n_3 L_3, \ \hat{\mathbf{p}}_{41} := \frac{1}{10^5} K^n_{41} L_4, \hat{\mathbf{p}}_{43} := \frac{1}{10^5} K^n_{43} L_4,$$
$$\hat{L}_3 := (\hat{\mathbf{p}}_{30}, \hat{\mathbf{p}}_{31}, \hat{\mathbf{p}}_{32}, \hat{\mathbf{p}}_{33})^T, \quad L_4 := (\mathbf{p}_{40}, \mathbf{p}_{41}, \mathbf{p}_{42}, \mathbf{p}_{43}, \mathbf{p}_{44})^T$$
$$L_3 := (\mathbf{p}_{30}, \mathbf{p}_{31}, \mathbf{p}_{32}, \mathbf{p}_{33}, \mathbf{p}_{34}, \mathbf{p}_{40}, \mathbf{p}_{41}, \mathbf{p}_{42}, \mathbf{p}_{43}, \mathbf{p}_{44})^T$$

and $\hat{\mathbf{p}}_{02}$, $\hat{\mathbf{p}}_{13}, \hat{\mathbf{p}}_{23}$ $\hat{\mathbf{p}}_{14}$ and $\hat{\mathbf{p}}_{34}$ are obtained symmetrically. The $\hat{\mathbf{p}}_{3j}$ and $\hat{\mathbf{p}}_{j3}$, $j = 0, 1, 2$, are used as target points when applying formula (7).

9.3. *Key formulas for cap^{bi5}*

With the notation of (15), $\hat{\mathbf{t}}^k_{i0}$, $i = 0, \dots, 5$ are the degree-raised boundary coefficients and

$$\hat{\mathbf{t}}^k_{01} := \bar{\mathbf{t}}^k_{00} + \frac{3a^k_0}{5} \dot{\mathbf{t}}^k_0, \ \hat{\mathbf{t}}^k_{11} := \frac{2}{5} \bar{\mathbf{t}}^k_{00} + \frac{3}{5} \bar{\mathbf{t}}^k_{10} + \frac{6a^k_1}{25} \dot{\mathbf{t}}^k_0 + \frac{9a^k_0}{25} \dot{\mathbf{t}}^k_1,$$
$$\hat{\mathbf{t}}^k_{21} := \frac{1}{10} \bar{\mathbf{t}}^k_{00} + \frac{3}{5} \bar{\mathbf{t}}^k_{10} + \frac{3}{10} \bar{\mathbf{t}}^k_{20} + \frac{3a^k_2}{50} \dot{\mathbf{t}}^k_0 + \frac{9a^k_1}{25} \dot{\mathbf{t}}^k_1 + \frac{9a^k_0}{50} \dot{\mathbf{t}}^k_2. \qquad (19)$$

The BB-coefficients $\hat{\mathbf{t}}^k_{5-k,1}$, $k = 0, 1, 2$, are obtained from $\hat{\mathbf{t}}_k$ by replacing $\bar{\mathbf{t}}^k_{ij}$ by $\bar{\mathbf{t}}^k_{3-i,j}$, and $\dot{\mathbf{t}}^k_i$ by $\dot{\mathbf{t}}^k_{3-i}$, and a^k_i by a^k_{2-i}. This yields cap$^{\text{bi5}}$ consisting of n internally C^1 2×2, G^1-connected sectors of degree bi-5 and so that the shape of cap$^{\text{aux}}$ is preserved and the cap$^{\text{bi5}}$ is smoothly (G^1) connected to the surrounding surface.

9.4. *Tables of cap^{aux} for $n = 3, 5, 7, 8, 9, 10$*

$$A^3_{33} := \begin{pmatrix} 3735 & 632 & -2084 & -2364 & 632 & -18746 & 2016 & 32437 & -2084 & 2016 & -2364 & 32437 \\ -2375 & -463 & 591 & 1449 & 663 & 11628 & -2072 & -13537 & 318 & -4796 & 1838 & -24860 \\ -2375 & 663 & 318 & 1838 & -463 & 11628 & -4796 & -24860 & 591 & -2072 & 1449 & -13537 \end{pmatrix},$$

$$A^3_{43} := \begin{pmatrix} 1099 & 931 & -1396 & -47 & -982 & -5424 & -214 & 10784 & 993 & 3340 & -2045 & 6941 \\ 1099 & -982 & 993 & -2045 & 931 & -5424 & 3340 & 6941 & -1396 & -214 & -47 & 10784 \\ -2199 & 50 & 402 & 2093 & 50 & 10848 & -3125 & -17726 & 402 & -3125 & 2093 & -17726 \end{pmatrix},$$

$$A^5_{33} := \begin{pmatrix} 2204 & 772 & -672 & -11013 & 772 & -18467 & 8745 & 27997 & -672 & 8745 & -11013 & 27997 \\ -17 & -1650 & 1314 & 405 & 2298 & -2062 & 7090 & -9026 & -681 & -4544 & -1446 & 8416 \\ -821 & -481 & -450 & 3525 & -978 & 8506 & -3961 & -7218 & 401 & -2854 & 5848 & -13513 \\ -821 & -978 & 401 & 5848 & -481 & 8506 & -2854 & -13513 & -450 & -3961 & 3525 & -7218 \\ -17 & 2298 & -681 & -1446 & -1650 & -2062 & -4544 & 8416 & 1314 & 7090 & 405 & -9026 \end{pmatrix},$$

$$A^5_{43} := \begin{pmatrix} 748 & 992 & -308 & -4082 & -77 & -7121 & 1589 & 11465 & 122 & 4806 & -3959 & 7485 \\ 748 & -77 & 122 & -3959 & 992 & -7121 & 4806 & 7485 & -308 & 1589 & -4082 & 11465 \\ -285 & -1040 & 384 & 1634 & 690 & 2720 & 1380 & -6839 & -313 & -3823 & 1436 & -398 \\ -925 & -565 & 114 & 4970 & -565 & 8802 & -3953 & -11712 & 114 & -3953 & 4970 & -11712 \\ -285 & 690 & -313 & 1436 & -1040 & 2720 & -3823 & -398 & 384 & 1380 & 1634 & -6839 \end{pmatrix},$$

$$A^7_{33} := \begin{pmatrix} 905 & 1420 & -947 & -12433 & 1420 & -13541 & 5533 & 26973 & -947 & 5533 & -12433 & 26973 \\ 316 & -115 & -676 & -3449 & 1746 & -6342 & 6191 & 5161 & 150 & -1238 & -7741 & 17950 \\ -347 & -667 & 48 & 3922 & 79 & 3540 & 272 & -9730 & 647 & -2805 & 3116 & -6235 \\ -219 & -816 & -144 & 3946 & -1045 & 5171 & -1558 & -7103 & -32 & -720 & 5210 & -9992 \\ -219 & -1045 & -32 & 5210 & -816 & 5171 & -720 & -9992 & -144 & -1558 & 3946 & -7103 \\ -347 & 79 & 647 & 3116 & -667 & 3540 & -2805 & -6235 & 48 & 272 & 3922 & -9730 \\ 316 & 1746 & 150 & -7741 & -115 & -6342 & -1238 & 17950 & -676 & 6191 & -3449 & 5161 \end{pmatrix},$$

$$A^7_{43} := \begin{pmatrix} 292 & 829 & -103 & -4892 & 512 & -5111 & 1133 & 10460 & -298 & 2418 & -4345 & 8610 \\ 292 & 512 & -298 & -4345 & 829 & -5111 & 2418 & 8610 & -103 & 1133 & -4892 & 10460 \\ 72 & -190 & -268 & -526 & 522 & -1262 & 1882 & 276 & 169 & -1005 & -1755 & 4433 \\ -202 & -750 & -36 & 3688 & -178 & 3537 & -70 & -8265 & 314 & -2387 & 2703 & -4932 \\ -324 & -744 & 222 & 5126 & -744 & 5673 & -1971 & -10583 & 222 & -1971 & 5126 & -10583 \\ -202 & -178 & 314 & 2703 & -750 & 3537 & -2387 & -4932 & -36 & -70 & 3688 & -8265 \\ 72 & 522 & 169 & -1755 & -190 & -1262 & -1005 & 4433 & -268 & 1882 & -526 & 276 \end{pmatrix},$$

$$A^8_{33} := \begin{pmatrix} 591 & 1414 & -860 & -12362 & 1414 & -11319 & 4266 & 25644 & -860 & 4266 & -12362 & 25644 \\ 277 & 284 & -878 & -4935 & 1547 & -6516 & 5087 & 8897 & 142 & -426 & -9092 & 19402 \\ -175 & -477 & -158 & 2850 & 355 & 1448 & 1261 & -7111 & 670 & -2423 & 673 & -1155 \\ -200 & -675 & 5 & 4149 & -760 & 4280 & -1154 & -7987 & 156 & -851 & 5227 & -10070 \\ -85 & -896 & -225 & 4187 & -896 & 3950 & -448 & -7135 & -225 & -448 & 4187 & -7135 \\ -200 & -760 & 156 & 5227 & -675 & 4280 & -851 & -10070 & 5 & -1154 & 4149 & -7987 \\ -175 & 355 & 670 & 673 & -477 & 1448 & -2423 & -1155 & -158 & 1261 & 2850 & -7111 \\ 277 & 1547 & 142 & -9092 & 284 & -6516 & -426 & 19402 & -878 & 5087 & -4935 & 8897 \end{pmatrix},$$

$$A^8_{43} := \begin{pmatrix} 188 & 740 & -81 & -4867 & 548 & -4258 & 889 & 9829 & -272 & 1740 & -4363 & 8453 \\ 188 & 548 & -272 & -4363 & 740 & -4258 & 1740 & 8453 & -81 & 889 & -4867 & 9829 \\ 78 & 34 & -304 & -1304 & 499 & -1763 & 1572 & 2125 & 157 & -482 & -2519 & 5447 \\ -78 & -499 & -157 & 2519 & -34 & 1763 & 482 & -5447 & 304 & -1572 & 1304 & -2125 \\ -188 & -740 & 81 & 4867 & -548 & 4258 & -889 & -9829 & 272 & -1740 & 4363 & -8453 \\ -188 & -548 & 272 & 4363 & -740 & 4258 & -1740 & -8453 & 81 & -889 & 4867 & -9829 \\ -78 & -34 & 304 & 1304 & -499 & 1763 & -1572 & -2125 & -157 & 482 & 2519 & -5447 \\ 78 & 499 & 157 & -2519 & 34 & -1763 & -482 & 5447 & -304 & 1572 & -1304 & 2125 \end{pmatrix},$$

$$A^9_{33} := \begin{pmatrix} 404 & 1348 & -759 & -12094 & 1348 & -9646 & 3377 & 24259 & -759 & 3377 & -12094 & 24259 \\ 227 & 509 & -892 & -6004 & 1397 & -6317 & 4166 & 11224 & 83 & 35 & -9742 & 19792 \\ -74 & -263 & -325 & 1500 & 511 & -42 & 1702 & -4014 & 620 & -1931 & -1405 & 2869 \\ -162 & -569 & 29 & 4103 & -473 & 3338 & -614 & -8175 & 311 & -1113 & 4369 & -8366 \\ -73 & -715 & -146 & 3788 & -828 & 3390 & -586 & -6376 & -176 & -88 & 4620 & -8060 \\ -73 & -828 & -176 & 4620 & -715 & 3390 & -88 & -8060 & -146 & -586 & 3788 & -6376 \\ -162 & -473 & 311 & 4369 & -569 & 3338 & -1113 & -8366 & 29 & -614 & 4103 & -8175 \\ -74 & 511 & 620 & -1405 & -263 & -42 & -1931 & 2869 & -325 & 1702 & 1500 & -4014 \\ 227 & 1397 & 83 & -9742 & 509 & -6317 & 35 & 19792 & -892 & 4166 & -6004 & 11224 \end{pmatrix},$$

$$A^9_{43} := \begin{pmatrix} 128 & 663 & -67 & -4736 & 538 & -3620 & 709 & 9204 & -230 & 1298 & -4305 & 8157 \\ 128 & 538 & -230 & -4305 & 663 & -3620 & 1298 & 8157 & -67 & 709 & -4736 & 9204 \\ 68 & 161 & -285 & -1860 & 478 & -1926 & 1280 & 3293 & 126 & -211 & -2951 & 5945 \\ -23 & -291 & -206 & 1455 & 68 & 669 & 662 & -3112 & 261 & -1033 & 215 & -96 \\ -104 & -607 & -31 & 4090 & -372 & 2951 & -264 & -8061 & 274 & -1372 & 3280 & -6092 \\ -136 & -639 & 158 & 4811 & -639 & 3852 & -1068 & -9238 & 158 & -1068 & 4811 & -9238 \\ -104 & -372 & 274 & 3280 & -607 & 2951 & -1372 & -6092 & -31 & -264 & 4090 & -8061 \\ -23 & 68 & 261 & 215 & -291 & 669 & -1033 & -96 & -206 & 662 & 1455 & -3112 \\ 68 & 478 & 126 & -2951 & 161 & -1926 & -211 & 5945 & -285 & 1280 & -1860 & 3293 \end{pmatrix},$$

$$A^{10}_{33} := \begin{pmatrix} 288 & 1265 & -667 & -11711 & 1265 & -8382 & 2750 & 22899 & -667 & 2750 & -11711 & 22899 \\ 183 & 630 & -836 & -6723 & 1276 & -5989 & 3446 & 12618 & 22 & 298 & -9969 & 19602 \\ -18 & -76 & -422 & 164 & 598 & -1052 & 1838 & -1121 & 534 & -1469 & -2996 & 5803 \\ -118 & -458 & -18 & 3677 & -240 & 2395 & -132 & -7429 & 403 & -1234 & 3100 & -5911 \\ -78 & -597 & -47 & 3766 & -690 & 3036 & -611 & -6599 & -53 & -189 & 4701 & -8364 \\ -34 & -709 & -226 & 3838 & -709 & 2773 & -59 & -6262 & -226 & -59 & 3838 & -6262 \\ -78 & -690 & -53 & 4701 & -597 & 3036 & -189 & -8364 & -47 & -611 & 3766 & -6599 \\ -118 & -240 & 403 & 3100 & -458 & 2395 & -1234 & -5911 & -18 & -132 & 3677 & -7429 \\ -18 & 598 & 534 & -2996 & -76 & -1052 & -1469 & 5803 & -422 & 1838 & 164 & -1121 \\ 183 & 1276 & 22 & -9969 & 630 & -5989 & 298 & 19602 & -836 & 3446 & -6723 & 12618 \end{pmatrix},$$

$$A^{10}_{43} := \begin{pmatrix} 90 & 598 & -57 & -4556 & 512 & -3140 & 578 & 8614 & -190 & 1002 & -4197 & 7802 \\ 90 & 512 & -190 & -4197 & 598 & -3140 & 1002 & 7802 & -57 & 578 & -4556 & 8614 \\ 56 & 231 & -250 & -2234 & 455 & -1940 & 1043 & 4010 & 96 & -66 & -3175 & 6135 \\ 0 & -138 & -214 & 581 & 138 & 0 & 686 & -1313 & 214 & -686 & -581 & 1313 \\ -56 & -455 & -96 & 3175 & -231 & 1940 & 66 & -6135 & 250 & -1043 & 2234 & -4010 \\ -90 & -598 & 57 & 4556 & -512 & 3140 & -578 & -8614 & 190 & -1002 & 4197 & -7802 \\ -90 & -512 & 190 & 4197 & -598 & 3140 & -1002 & -7802 & 57 & -578 & 4556 & -8614 \\ -56 & -231 & 250 & 2234 & -455 & 1940 & -1043 & -4010 & -96 & 66 & 3175 & -6135 \\ 0 & 138 & 214 & -581 & -138 & 0 & -686 & 1313 & -214 & 686 & 581 & -1313 \\ 56 & 455 & 96 & -3175 & 231 & -1940 & -66 & 6135 & -250 & 1043 & -2234 & 4010 \end{pmatrix},$$

9.5. Tables of $cap^{\boxplus}$ for $n = 3, 5, 7, 8, 9, 10$

$$K^3_{00} := \begin{pmatrix} 327 & 1368 & 2144 & 1493 & 389 \\ 1368 & 5717 & 8958 & 6238 & 1628 \\ 2144 & 8958 & 14035 & 9773 & 2552 \\ 1493 & 6238 & 9773 & 6805 & 1777 \\ 389 & 1628 & 2552 & 1777 & 476 \end{pmatrix}, \; K^3_{10} := \begin{pmatrix} -20 & 592 & 1992 & 2128 & 749 \\ -53 & 2613 & 8540 & 9042 & 3169 \\ -32 & 4309 & 13717 & 14402 & 5027 \\ 13 & 3150 & 9787 & 10193 & 3543 \\ 12 & 861 & 2617 & 2704 & 945 \end{pmatrix},$$

$$K^3_{20} := \begin{pmatrix} 5 & -35 & 1043 & 2638 & 1409 \\ 17 & -86 & 4946 & 11532 & 6066 \\ 19 & -29 & 8772 & 18747 & 9834 \\ 8 & 58 & 6902 & 13411 & 7143 \\ 1 & 36 & 2034 & 3552 & 1977 \end{pmatrix}, K^3_{11} := \begin{pmatrix} -4 & -48 & -73 & -13 & 15 \\ -48 & 1078 & 3911 & 4419 & 1635 \\ -73 & 3911 & 13074 & 14173 & 5086 \\ -13 & 4419 & 14173 & 15080 & 5340 \\ 15 & 1635 & 5086 & 5340 & 1882 \end{pmatrix},$$

$$K^3_{21} := \begin{pmatrix} 2 & -4 & -98 & -112 & 36 \\ 17 & -72 & 1963 & 5275 & 3111 \\ 32 & -94 & 7789 & 17993 & 9776 \\ 20 & 26 & 9517 & 19650 & 10484 \\ 4 & 53 & 3804 & 7016 & 3812 \end{pmatrix}, K^3_{22} := \begin{pmatrix} 327 & 1368 & 2144 & 1493 & 389 \\ 1368 & 5717 & 8958 & 6238 & 1628 \\ 2144 & 8958 & 14035 & 9773 & 2552 \\ 1493 & 6238 & 9773 & 6805 & 1777 \\ 389 & 1628 & 2552 & 1777 & 476 \end{pmatrix},$$

$$K^3_{3} := \begin{pmatrix} 2005 & 9796 & 17942 & 14605 & 4458 & 2591 & 11572 & 19213 & 14025 & 3793 \\ -180 & 3913 & 15948 & 20129 & 8326 & -111 & 5309 & 18508 & 20636 & 7522 \\ 87 & -207 & 8362 & 24122 & 14316 & 102 & 30 & 12469 & 24362 & 16357 \\ 0 & 0 & 0 & 19112 & 27518 & 0 & 0 & 0 & 27518 & 25852 \end{pmatrix},$$

$$K^3_{41} := \begin{pmatrix} -312 & 8294 & 33180 & 41653 & 17185 \end{pmatrix}, \; K^3_{43} := \begin{pmatrix} 0 & 0 & 0 & 43718 & 56282 \end{pmatrix},$$

$$K^5_{00} := \begin{pmatrix} 459 & 1764 & 2539 & 1625 & 389 \\ 1764 & 6773 & 9751 & 6239 & 1497 \\ 2539 & 9751 & 14038 & 8982 & 2155 \\ 1625 & 6239 & 8982 & 5747 & 1379 \\ 389 & 1497 & 2155 & 1379 & 343 \end{pmatrix}, \; K^5_{10} := \begin{pmatrix} 25 & 982 & 2688 & 2536 & 804 \\ 62 & 3639 & 10133 & 9615 & 3058 \\ 40 & 5050 & 14316 & 13669 & 4361 \\ -5 & 3110 & 8986 & 8635 & 2764 \\ -8 & 717 & 2114 & 2045 & 664 \end{pmatrix},$$

$$K^5_{20} := \begin{pmatrix} -6 & 40 & 2079 & 3563 & 1675 \\ -19 & 90 & 7412 & 13312 & 6286 \\ -18 & 43 & 9900 & 18606 & 8852 \\ -4 & -25 & 5871 & 11533 & 5542 \\ 0 & -17 & 1304 & 2675 & 1306 \end{pmatrix}, \; K^5_{11} := \begin{pmatrix} 8 & 62 & 86 & 21 & -10 \\ 62 & 2071 & 5427 & 4915 & 1496 \\ 86 & 5427 & 14874 & 13861 & 4326 \\ 21 & 4915 & 13861 & 13098 & 4130 \\ -10 & 1496 & 4326 & 4130 & 1321 \end{pmatrix},$$

$$K^5_{21} := \begin{pmatrix} -2 & 12 & 139 & 132 & -50 \\ -18 & 93 & 4273 & 7115 & 3075 \\ -30 & 113 & 10755 & 19222 & 8900 \\ -14 & 7 & 9373 & 17678 & 8418 \\ 0 & -25 & 2747 & 5440 & 2647 \end{pmatrix}, K^5_{22} := \begin{pmatrix} 459 & 1764 & 2539 & 1625 & 389 \\ 1764 & 6773 & 9751 & 6239 & 1497 \\ 2539 & 9751 & 14038 & 8982 & 2155 \\ 1625 & 6239 & 8982 & 5747 & 1379 \\ 389 & 1497 & 2155 & 1379 & 343 \end{pmatrix},$$

$$K^5_{3} := \begin{pmatrix} 4154 & 14586 & 19206 & 11240 & 2466 & 3553 & 13105 & 18084 & 11067 & 2539 \\ 241 & 8306 & 20760 & 17897 & 5189 & 118 & 6932 & 18553 & 16869 & 5135 \\ -106 & 281 & 15935 & 26175 & 10992 & -74 & 78 & 13051 & 23203 & 10465 \\ 0 & 0 & 0 & 29478 & 24419 & 0 & 0 & 0 & 24419 & 21684 \end{pmatrix},$$

$$K^5_{41} := \begin{pmatrix} 351 & 15675 & 39657 & 34337 & 9980 \end{pmatrix}, \; K^5_{43} := \begin{pmatrix} 0 & 0 & 0 & 54293 & 45707 \end{pmatrix},$$

$$K^7_{00} := \begin{pmatrix} 570 & 2071 & 2819 & 1705 & 386 \\ 2071 & 7519 & 10234 & 6191 & 1404 \\ 2819 & 10234 & 13930 & 8426 & 1911 \\ 1705 & 6191 & 8426 & 5097 & 1156 \\ 386 & 1404 & 1911 & 1156 & 278 \end{pmatrix}, \; K^7_{10} := \begin{pmatrix} 68 & 1298 & 3194 & 2795 & 829 \\ 158 & 4382 & 11143 & 9873 & 2950 \\ 92 & 5515 & 14555 & 13069 & 3931 \\ -18 & 3064 & 8434 & 7681 & 2327 \\ -21 & 633 & 1829 & 1691 & 528 \end{pmatrix},$$

$$K^7_{20} := \begin{pmatrix} -17 & 109 & 2848 & 4225 & 1788 \\ -52 & 218 & 8904 & 14426 & 6232 \\ -47 & 83 & 10401 & 18315 & 8131 \\ -9 & -63 & 5374 & 10262 & 4703 \\ 3 & -36 & 1035 & 2143 & 1024 \end{pmatrix}, \; K^7_{11} := \begin{pmatrix} 27 & 173 & 214 & 40 & -28 \\ 173 & 2845 & 6433 & 5165 & 1398 \\ 214 & 6433 & 15834 & 13485 & 3860 \\ 40 & 5165 & 13485 & 11836 & 3468 \\ -28 & 1398 & 3860 & 3468 & 1042 \end{pmatrix},$$

$$K^7_{21} := \begin{pmatrix} -5 & 44 & 398 & 355 & -169 \\ -47 & 258 & 5913 & 8324 & 2911 \\ -80 & 263 & 12371 & 19706 & 8235 \\ -36 & -1 & 9225 & 16207 & 7274 \\ 0 & -55 & 2324 & 4471 & 2114 \end{pmatrix}, \; K^7_{22} := \begin{pmatrix} 570 & 2071 & 2819 & 1705 & 386 \\ 2071 & 7519 & 10234 & 6191 & 1404 \\ 2819 & 10234 & 13930 & 8426 & 1911 \\ 1705 & 6191 & 8426 & 5097 & 1156 \\ 386 & 1404 & 1911 & 1156 & 278 \end{pmatrix},$$

$$K^7_{3} := \begin{pmatrix} 5597 & 16996 & 19351 & 9792 & 1858 & 4172 & 13853 & 17124 & 9349 & 1908 \\ 680 & 11025 & 22752 & 16674 & 4143 & 316 & 7810 & 18117 & 14556 & 3927 \\ -268 & 847 & 20393 & 27246 & 9124 & -176 & 236 & 13699 & 20608 & 8291 \\ 0 & 0 & 0 & 35036 & 23730 & 0 & 0 & 0 & 23730 & 17504 \end{pmatrix},$$

$$K^7_{41} := \begin{pmatrix} 942 & 19576 & 41319 & 30538 & 7625 \end{pmatrix}, \; K^7_{43} := \begin{pmatrix} 0 & 0 & 0 & 59191 & 40809 \end{pmatrix},$$

$$K^8_{00} := \begin{pmatrix} 611 & 2180 & 2913 & 1730 & 385 \\ 2180 & 7770 & 10383 & 6167 & 1373 \\ 2913 & 10383 & 13876 & 8241 & 1835 \\ 1730 & 6167 & 8241 & 4894 & 1090 \\ 385 & 1373 & 1835 & 1090 & 255 \end{pmatrix}, \; K^8_{10} := \begin{pmatrix} 85 & 1413 & 3368 & 2879 & 837 \\ 193 & 4635 & 11467 & 9942 & 2911 \\ 107 & 5657 & 14606 & 12860 & 3796 \\ -25 & 3041 & 8248 & 7384 & 2198 \\ -25 & 606 & 1742 & 1588 & 487 \end{pmatrix},$$

$$K^8_{20} := \begin{pmatrix} -22 & 135 & 3117 & 4468 & 1814 \\ -65 & 262 & 9370 & 14796 & 6195 \\ -57 & 90 & 10514 & 18193 & 7900 \\ -10 & -78 & 5209 & 9858 & 4457 \\ 4 & -42 & 959 & 1988 & 945 \end{pmatrix}, \; K^8_{11} := \begin{pmatrix} 35 & 217 & 258 & 43 & -35 \\ 217 & 3121 & 6762 & 5230 & 1363 \\ 258 & 6762 & 16113 & 13340 & 3714 \\ 43 & 5230 & 13340 & 11437 & 3272 \\ -35 & 1363 & 3714 & 3272 & 966 \end{pmatrix},$$

$$K^8_{21} := \begin{pmatrix} -6 & 60 & 504 & 442 & -222 \\ -58 & 323 & 6470 & 8739 & 2835 \\ -98 & 311 & 12837 & 19825 & 8019 \\ -43 & -11 & 9138 & 15721 & 6936 \\ 1 & -66 & 2198 & 4184 & 1961 \end{pmatrix}, \; K^8_{22} := \begin{pmatrix} 611 & 2180 & 2913 & 1730 & 385 \\ 2180 & 7770 & 10383 & 6167 & 1373 \\ 2913 & 10383 & 13876 & 8241 & 1835 \\ 1730 & 6167 & 8241 & 4894 & 1090 \\ 385 & 1373 & 1835 & 1090 & 255 \end{pmatrix},$$

$$K^8_{3} := \begin{pmatrix} 6081 & 17693 & 19303 & 9359 & 1701 & 4395 & 14093 & 16800 & 8837 & 1738 \\ 857 & 11902 & 23250 & 16250 & 3859 & 394 & 8103 & 17943 & 13849 & 3593 \\ -320 & 1089 & 21845 & 27491 & 8506 & -211 & 301 & 13886 & 19729 & 7684 \\ 0 & 0 & 0 & 36829 & 23491 & 0 & 0 & 0 & 23491 & 16189 \end{pmatrix},$$

$$K^8_{41} := \begin{pmatrix} 1172 & 20789 & 41640 & 29383 & 7016 \end{pmatrix}, \; K^8_{43} := \begin{pmatrix} 0 & 0 & 0 & 60687 & 39313 \end{pmatrix}.$$

$$K^9_{00} := \begin{pmatrix} 644 & 2266 & 2986 & 1748 & 384 \\ 2266 & 7963 & 10493 & 6146 & 1349 \\ 2986 & 10493 & 13828 & 8099 & 1778 \\ 1748 & 6146 & 8099 & 4743 & 1041 \\ 384 & 1349 & 1778 & 1041 & 242 \end{pmatrix}, \; K^9_{10} := \begin{pmatrix} 100 & 1505 & 3505 & 2943 & 842 \\ 220 & 4831 & 11712 & 9989 & 2881 \\ 118 & 5762 & 14636 & 12697 & 3694 \\ -31 & 3020 & 8105 & 7163 & 2103 \\ -29 & 585 & 1677 & 1513 & 459 \end{pmatrix},$$

$$K^9_{20} := \begin{pmatrix} -25 & 158 & 3328 & 4663 & 1831 \\ -75 & 295 & 9719 & 15082 & 6162 \\ -66 & 93 & 10583 & 18089 & 7727 \\ -12 & -91 & 5081 & 9554 & 4277 \\ 4 & -46 & 904 & 1876 & 889 \end{pmatrix}, \; K^9_{11} := \begin{pmatrix} 43 & 253 & 292 & 44 & -40 \\ 253 & 3340 & 7012 & 5275 & 1335 \\ 292 & 7012 & 16315 & 13222 & 3605 \\ 44 & 5275 & 13222 & 11138 & 3130 \\ -40 & 1335 & 3605 & 3130 & 908 \end{pmatrix},$$

$$K^9_{21} := \begin{pmatrix} -6 & 74 & 592 & 515 & -268 \\ -67 & 377 & 6903 & 9062 & 2771 \\ -114 & 346 & 13173 & 19902 & 7856 \\ -50 & -21 & 9057 & 15346 & 6690 \\ 2 & -74 & 2104 & 3974 & 1856 \end{pmatrix}, \; K^9_{22} := \begin{pmatrix} 644 & 2266 & 2986 & 1748 & 384 \\ 2266 & 7963 & 10493 & 6146 & 1349 \\ 2986 & 10493 & 13828 & 8099 & 1778 \\ 1748 & 6146 & 8099 & 4743 & 1041 \\ 384 & 1349 & 1778 & 1041 & 242 \end{pmatrix},$$

$$K^9_{3} := \begin{pmatrix} 6456 & 18199 & 19238 & 9038 & 1592 & 4574 & 14275 & 16550 & 8461 & 1617 \\ 1005 & 12572 & 23583 & 15916 & 3656 & 460 & 8329 & 17801 & 13324 & 3354 \\ -357 & 1298 & 22995 & 27610 & 8030 & -239 & 354 & 14008 & 19047 & 7254 \\ 0 & 0 & 0 & 38278 & 23265 & 0 & 0 & 0 & 23265 & 15192 \end{pmatrix},$$

$$K^9_{41} := \begin{pmatrix} 1364 & 21705 & 41823 & 28518 & 6590 \end{pmatrix}, K^9_{43} := \begin{pmatrix} 0 & 0 & 0 & 61869 & 38131 \end{pmatrix}.$$

$$K^{10}_{00} := \begin{pmatrix} 671 & 2334 & 3042 & 1762 & 383 \\ 2334 & 8114 & 10577 & 6128 & 1331 \\ 3042 & 10577 & 13788 & 7988 & 1735 \\ 1762 & 6128 & 7988 & 4628 & 1005 \\ 383 & 1331 & 1735 & 1005 & 229 \end{pmatrix}, \; K^{10}_{10} := \begin{pmatrix} 111 & 1579 & 3613 & 2993 & 845 \\ 242 & 4986 & 11900 & 10023 & 2857 \\ 126 & 5841 & 14654 & 12568 & 3616 \\ -36 & 3002 & 7992 & 6993 & 2032 \\ -31 & 569 & 1628 & 1456 & 441 \end{pmatrix},$$

$$K^{10}_{20} := \begin{pmatrix} -28 & 176 & 3496 & 4822 & 1841 \\ -83 & 321 & 9986 & 15305 & 6134 \\ -73 & 94 & 10627 & 18003 & 7594 \\ -12 & -101 & 4979 & 9318 & 4142 \\ 5 & -49 & 863 & 1793 & 847 \end{pmatrix}, \; K^{10}_{11} := \begin{pmatrix} 49 & 283 & 319 & 44 & -45 \\ 283 & 3516 & 7207 & 5306 & 1313 \\ 319 & 7207 & 16465 & 13126 & 3520 \\ 44 & 5306 & 13126 & 10907 & 3023 \\ -45 & 1313 & 3520 & 3023 & 871 \end{pmatrix},$$

$$K^{10}_{21} := \begin{pmatrix} -7 & 86 & 666 & 576 & -307 \\ -75 & 422 & 7244 & 9320 & 2717 \\ -126 & 372 & 13422 & 19955 & 7730 \\ -55 & -31 & 8987 & 15053 & 6504 \\ 2 & -81 & 2032 & 3816 & 1778 \end{pmatrix}, \; K^{10}_{22} := \begin{pmatrix} 671 & 2334 & 3042 & 1762 & 383 \\ 2334 & 8114 & 10577 & 6128 & 1331 \\ 3042 & 10577 & 13788 & 7988 & 1735 \\ 1762 & 6128 & 7988 & 4628 & 1005 \\ 383 & 1331 & 1735 & 1005 & 229 \end{pmatrix},$$

$$K^{10}_{3} := \begin{pmatrix} 6750 & 18577 & 19172 & 8793 & 1512 & 4719 & 14417 & 16354 & 8177 & 1529 \\ 1127 & 13090 & 23816 & 15651 & 3505 & 515 & 8509 & 17685 & 12923 & 3179 \\ -386 & 1472 & 23874 & 27715 & 7639 & -260 & 400 & 14109 & 18497 & 6940 \\ 0 & 0 & 0 & 39372 & 23110 & 0 & 0 & 0 & 23110 & 14408 \end{pmatrix},$$

$$K^{10}_{41} := \begin{pmatrix} 1522 & 22410 & 41932 & 27858 & 6278 \end{pmatrix}, \; K^{10}_{43} := \begin{pmatrix} 0 & 0 & 0 & 62747 & 37253 \end{pmatrix}.$$